Sensing and Communication Optimal Trade-Off for MIMO Bistatic Systems

Flavio Zabini, *Member, IEEE*, and Andrea Giorgetti, *Senior Member, IEEE*

***Abstract*—To enable mobile perceptive networks, two critical components are essential: the adoption of bistatic configurations that eliminate the need for full-duplex technology and the development of methodologies to balance localization and communication functionalities under respective constraints.Addressing these challenges, this work investigates a joint sensing communication (JSC) multiple input-multiple output (MIMO) system employing a bistatic sensing configuration for target localization. We develop an analytical framework to derive both exact and low-complexity suboptimal solutions for the beamforming weight vector, minimizing localization error while adhering to communication and power constraints. This framework establishes fundamental limits for JSC MIMO systems operating in bistatic mode, offering valuable insights into target localization performance as a function of the required communication signal-to-noise ratio (SNR). Numerical results validate the proposed methodology, demonstrating its effectiveness in optimizing sensing performance across a specified area of interest while maintaining compliance with communication constraints for users.**

***Index Terms*—Joint sensing and communication, multiple antennas, Cramér-Rao bound, Fisher information, localization error, optimal beamforming.**

I. Introduction

THE integration of sensing and communication functionalities has emerged as a pivotal area of research, driven by the growing demand for Internet of Things (IoT) applications [2], [3] and the rapid evolution of next-generation 6G mobile networks [4], [5], [6], [7], [8], [9], [10], [11]. Emerging applications such as perceptive mobile networks [12], intelligent transportation systems [13], enhanced safety measures [14], assisted living technologies, human-machine interfaces, broadcasting services [15], and mobile crowdsensing [16], [17] demand systems capable of achieving seamless coexistence between sensing and communication [18], [19], [20], [21], [22], [23], [24], [25], [26], [27], [28].

Received 11 May 2025; revised 23 July 2025; accepted 24 August 2025. Date of publication 10 September 2025; date of current version 6 March 2026. This work was supported in part by the Consorzio Nazionale Interuniversitario per le Telecomunicazioni National Laboratory WiLab and the WiLab-Huawei Joint Innovation Center, and in part by the European Union under the Italian National Recovery and Resilience Plan of NextGenerationEU, partnership on "Telecommunications of the Future" (PE00000001 - program "RESTART"). An earlier version of this paper was presented in part at the International Conference on Communications (ICC) Workshops, Rome, Italy, June 2023 [DOI: 10.1109/ICCWorkshops57953.2023.10283688]. The review of this article was coordinated by Dr. Cunhua Pan. *(Corresponding author: Flavio Zabini.)*

The authors are with the Department of Electrical, Electronic, and Information Engineering "Guglielmo Marconi" (DEI), CNIT, University of Bologna, 40136 Bologna, Italy (e-mail: flavio.zabini2@unibo.it; andrea.giorgetti@unibo.it).

Digital Object Identifier 10.1109/TVT.2025.3608462

With advancements in automation, the need for precise vehicle positioning has become critical, enabling autonomous navigation in increasingly complex environments. Such precision relies on leveraging mobile networks to sense the environment [29], including vehicles and pedestrians, while vehicle-to-everything (V2X) sidelink communication, a powerful enabler for localization tasks, enhances the capabilities of modern vehicular networks [30], [31], [32], [33].

Recent solutions have explored different strategies to enhance joint sensing and communication (JSC) capabilities [34], [35], [36], [37], [38], [39]. For instance, active reconfigurable intelligent surfaces have been shown to improve radar signal-to-interference plus noise ratio (SINR) through joint optimization of transmit and reflection parameters while maintaining communication quality of service constraints [40]. On the receiver side, projection-based schemes have been proposed to mitigate mutual interference between uplink signal detection and sensing tasks, enabling simultaneous high-performance operation through joint multi-snapshot processing [41].

To fully exploit the efficiency of integrating these two functionalities, it is essential to design a flexible waveform that appropriately balances the trade-off between sensing and communication [42], [43], [44], [45], [46]. Recent advancements in multiple-input multiple-output (MIMO) technology have demonstrated significant benefits on the communication side, such as spatial diversity, increased capacity, and robust mitigation of channel fading. Additionally, MIMO introduces degrees of freedom to accommodate and enhance sensing performance [47], [48], [49], [50], [51]. In a MIMO setup, this trade-off manifests itself in the conflicting requirements of beamforming patterns: communication performance demands beam design that maximizes the signal-to-noise ratio (SNR) for the user equipment (UE), while sensing performance is maximized by focusing transmitted power toward the target for detection or localization.

Several recent works have explored the JSC trade-off. For example, [52] examines a monostatic MIMO base station (BS) detecting a single target while transmitting data to multiple users. An analytical expression for the JSC trade-off (detection probability vs. bit rate) is provided, though it remains unclear whether the proposed dual-function waveform achieves theoretical limits. Similarly, [53] evaluates the Cramér-Rao Bound (CRB) for target direction estimation in a monostatic setup, deriving the optimal trade-off between the CRB and communication SNR. The finite block-length regime's impact on the JSC trade-off is addressed in [54].

However, many studies assume monostatic radar configurations [55], [56], [57], where the BS transmitting the dual-function waveform also performs sensing using full-duplex technology [22]. This approach presents practical challenges due to

weak reflected signals from targets. Additionally, monostatic configurations are restrictive in scenarios requiring cooperation between multiple BSs. Consequently, investigating the JSC trade-off in a bistatic setting becomes crucial for understanding its potential in networked environments [1], [58], [59], [60], [61]. Recent efforts have introduced bistatic JSC systems using orthogonal frequency-division multiplexing [62], standardized 5G New Radio waveforms [63], and integrated multiuser beamforming designs [64]. Despite these advancements, key questions remain unanswered, particularly regarding the analytical derivation of CRB for target position estimation in a bistatic system integrated with communication. Existing works do not jointly optimize beamforming for sensing and communication functionalities, leaving a significant gap in understanding the potential of bistatic JSC systems. This work addresses these gaps by:

- Deriving explicit analytical expressions for the CRB of target position estimation in a MIMO bistatic configuration with transmit beamforming.
- Providing an exact solution for the optimal beamforming weight vector to maximize localization performance while satisfying power and SNR constraints in the single user case.
- Proposing suboptimal beamforming strategies that closely approximate the optimal solution without requiring complex optimization procedures.
- Proposing an optimal design strategy for the beamforming weight vector is derived to maximize localization performance under power and SINR constraints in the multi-user case, leveraging semi-definite programming (SDP).
- Analyzing the JSC trade-off in both non-line-of-sight (NLoS) and line-of-sight (LoS) scenarios, incorporating the effects of channel randomness.
- Demonstrating that optimal beamforming substantially reduces the CRB across the area of interest while meeting communication constraints, thereby validating the effectiveness of the proposed methodology.

Throughout the paper, capital boldface letters denote matrices, lowercase bold letters denote vectors, with $\mathbf{v}_j$ we represent the jth column of the matrix $\mathbf{V}$, $(\cdot)^{\mathsf{T}}$ stands for transposition, $(\cdot)^{\mathsf{H}}$ stands for Hermitian transposition, $\mathbf{I}_n$ is the $n \times n$ identity matrix, $\mathbf{0}_n$ is the vector of n zeros, $||\cdot||$ is the l_2-norm, $\mathrm{tr}(\cdot)$ is the trace of a matrix, $\nabla[\cdot]$ represents the gradient, $|\cdot|$ is the absolute value, $\Re\{\cdot\}$ is the real part of a complex number, and $\mathbb{E}\{\cdot\}$ denotes the expectation operator.

The rest of the paper is organized as follows. In Section II, the scenario and the system model are introduced. Section III derives the CRB of position estimation. Section IV analyzes the JSC trade-off, deriving both optimal and suboptimal solutions. Numerical results are given in Section V. Conclusion are drawn in section VI.

II. System Model

Let us consider a dual-function system that combines communication and sensing capabilities within a bistatic radar configuration, as illustrated in Fig. 1. In this particular arrangement, both the transmitter and the receiver are equipped with antenna arrays comprising N_{T} and N_{R} elements, respectively, with N_{T} being less than N_{R}. In this context, the transmitted signal serves a dual purpose: it handles communication by delivering information to a single antenna UE while simultaneously illuminating a target

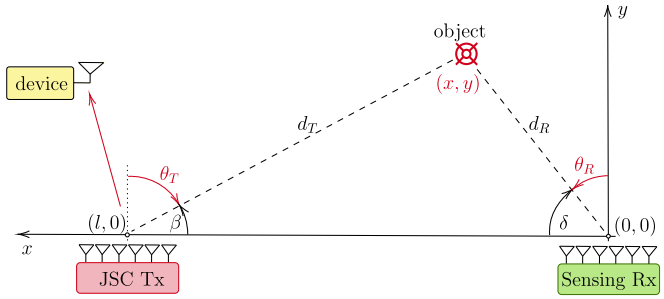

Fig. 1. The dual-function system with communication and bistatic radar capabilities.

for radar purposes. The bistatic pair, consisting of a transmitter and a receiver, is responsible for determining the target's position, distinct from that of the UE, all the while ensuring a predefined level of communication quality for the UE.

To exemplify the scenario, we consider the transmitter (Tx) and receiver (Rx) to be two BSs, one operating in downlink and the other listening to the transmitted signal scattered by the target, both cooperating to perform JSC; however, the Rx can be a specific device used for sensing purposes only. In the system under consideration, position estimation relies exclusively on measuring the angles of arrival and departure. Furthermore, as in [9], we consider the general case with K communication users, providing an analytical solution for $K = 1$ (single user) and a SDP-based solution for $K > 1$ (multiuser case). The rationale behind this distinction is to preserve an analytical solution for the specific single-user case while simultaneously enabling a semi-analytical solution for the general case.

The dual-function waveform emitted by the Tx consists of L symbols and is represented as a $N_{\mathrm{T}} \times L$ matrix $\mathbf{X}$ whose (i,j)-th element is the discrete signal sample transmitted at the i-th antenna in the j-th time slot.[1] In particular, we consider:

$$\mathbf{X} = \mathbf{W}_{\mathrm{DF}}\, \mathbf{S}_{\mathrm{C}}^{\mathsf{H}} \tag{1}$$

where $\mathbf{W}_{\mathrm{DF}} \triangleq (\mathbf{w}_1, \mathbf{w}_2, \ldots, \mathbf{w}_K) \in \mathbb{C}^{N_{\mathrm{T}} \times K}$ is the dual function beamforming matrix to be optimized, being $\mathbf{w}_k \triangleq (w_1^{(k)}, w_2^{(k)}, \ldots, w_{N_{\mathrm{T}}}^{(k)})^{\mathsf{T}} \in \mathbb{C}^{N_{\mathrm{T}} \times 1}$ the weight vector related to the k-th user (with $k = 1, 2, \ldots, K$) and $\mathbf{S}_{\mathrm{C}} = (\mathbf{s}_{\mathrm{C}1}, \mathbf{s}_{\mathrm{C}2}, \ldots, \mathbf{s}_{\mathrm{C}K}) \in \mathbb{C}^{K \times L}$ is the signal matrix whose k-th row $\mathbf{s}_{\mathrm{C}k} \triangleq (s_1^{(k)}, s_2^{(k)}, \ldots, s_L^{(k)})^{\mathsf{T}} \in \mathbb{C}^{L \times 1}$ contains the zero mean (i.e., $\mathbb{E}\{s_i^{(k)}\} = 0$ for $i = 1, 2, \ldots, L$) unit power data stream of symbols related to the k-th user, so that $\mathbf{s}_{\mathrm{C}k}^{\mathsf{H}} \mathbf{s}_{\mathrm{C}k} = L$ for all k and $\mathbf{S}_{\mathrm{C}} \mathbf{S}_{\mathrm{C}}^{H} = L\mathbf{I}_K$ (being $\mathbf{I}_K$ the $K \times K$ identity matrix). Under these assumptions, the covariance matrix is

$$\mathbf{R}_{\mathrm{X}} \triangleq \frac{1}{L}\mathbf{X}\mathbf{X}^{\mathsf{H}} = \frac{1}{L}\mathbf{W}_{\mathrm{DF}}\mathbf{S}_{\mathrm{C}}^{\mathsf{H}}\mathbf{S}_{\mathrm{C}}\mathbf{W}_{\mathrm{DF}}^{\mathsf{H}} = \mathbf{W}_{\mathrm{DF}}\mathbf{W}_{\mathrm{DF}}^{\mathsf{H}} \tag{2}$$

and, by indicating as $\|\cdot\|_F$ the Frobenius norm, the transmission power constraint results in

$$\frac{1}{L}\sum_{i=1}^{N_{\mathrm{T}}}\sum_{j=1}^{L}|x_{ij}|^2 = \frac{1}{L}\mathrm{tr}(\mathbf{X}\mathbf{X}^{\mathsf{H}}) = \mathrm{tr}(\mathbf{W}_{\mathrm{DF}}\mathbf{W}_{\mathrm{DF}}^{\mathsf{H}})$$

$$= \|\mathbf{W}_{\mathrm{DF}}\|_F^2 \leq P_{\mathrm{T}} \tag{3}$$

[1] Without loss of generality, the baseband representation of signals is considered.

where P_{T} is the maximum transmit power.

A. Communication Functionality

By denoting as $\mathbf{y}_{\mathrm{C}k} = (y_1^{(k)}, y_2^{(k)}, \ldots, y_L^{(k)})^{\mathsf{T}} \in \mathbb{C}^{L\times 1}$ the signal received by the k-th UE, the received signal matrix $\mathbf{Y}_{\mathrm{C}} \triangleq (\mathbf{y}_{\mathrm{C}1}, \mathbf{y}_{\mathrm{C}2}, \ldots, \mathbf{y}_{\mathrm{C}K}) \in \mathbb{C}^{L\times K}$ can be written as

$$\mathbf{Y}_{\mathrm{C}} = \mathbf{X}^{\mathsf{H}}\mathbf{H} + \mathbf{Z}_{\mathrm{C}} \tag{4}$$

where $\mathbf{H} \triangleq (\mathbf{h}_1, \mathbf{h}_2, \ldots, \mathbf{h}_K)$ is the $N_{\mathrm{T}} \times K$ communication channel matrix, being $\mathbf{h}_k \triangleq (h_1, h_2, \ldots, h_{N_{\mathrm{T}}})^{\mathsf{T}} \in \mathbb{C}^{N_{\mathrm{T}}\times 1}$ the vector of the channel coefficients related to the k-th communication user and $\mathbf{Z}_{\mathrm{C}} \triangleq (\mathbf{z}_{\mathrm{C}1}, \mathbf{z}_{\mathrm{C}2}, \ldots, \mathbf{z}_{\mathrm{C}K}) \in \mathbb{C}^{L\times K}$ is the noise matrix, being $\mathbf{z}_{\mathrm{C}k} \triangleq (z_1^{(k)}, z_2^{(k)}, \ldots, z_L^{(k)})^{\mathsf{T}} \in \mathbb{C}^{L\times 1}$ the additive white Gaussian noise (AWGN) vector for the k-th communication user with independent, identically distributed (i.i.d.) components and $\mathbb{E}\{|z_j|^2\} = \sigma_{\mathrm{C}}^2$ for $j = 1, 2, \ldots, L$. The SINRfor the k-th communication user is thus given by

$$\gamma_k = \frac{\|\mathbf{s}_{\mathrm{C}k}\mathbf{w}_k^{\mathsf{H}}\mathbf{h}_k\|^2}{\sum_{\substack{i=1\\ i\neq k}}^{K} \|\mathbf{s}_{\mathrm{C}i}\mathbf{w}_i^{\mathsf{H}}\mathbf{h}_k\|^2 + L\sigma_{\mathrm{C}}^2} = \frac{|\mathbf{h}_k^{\mathsf{H}}\mathbf{w}_k|^2}{\sum_{\substack{i=1\\ i\neq k}}^{K} |\mathbf{h}_k^{\mathsf{H}}\mathbf{w}_i|^2 + \sigma_{\mathrm{C}}^2}\,. \tag{5}$$

B. Bistatic Sensing Functionality

Regarding the radar functionality, the bistatic configuration is represented by the angle of departure (AoD) θ_{T} and angle of arrival (AoA) θ_{R} of the target and the baseline l. In this setting, let us denote with d_{T} and d_{R} the distance of the target from the Tx and the Rx, respectively. By considering the radar equation in free space propagation,[2] we can define the reflection coefficient α taking both the path-loss and the radar cross-section (RCS) of the target, σ_{rcs}, into account such that [65]

$$|\alpha|^2 = \frac{G_{\mathrm{T}}G_{\mathrm{R}}\lambda^2\sigma_{\mathrm{rcs}}}{(4\pi)^3 d_{\mathrm{T}}^2 d_{\mathrm{R}}^2} \tag{6}$$

where G_{T} and G_{R} are the gain of the array elements at the Tx and Rx, $\lambda = c/f_{\mathrm{c}}$ is the wavelength associated with the transmitted signal, c is the speed of light, and f_{c} is the carrier frequency.

For the radar purpose, the element $x_{i,j}$ of $\mathbf{X}$ is the j-th fast-time snapshot transmitted at the i-th antenna [52], [53]. Therefore, we can write the reflected echo signal as an $N_{\mathrm{R}} \times L$ matrix

$$\mathbf{Y}_{\mathrm{R}} = \alpha\mathbf{A}_{\mathrm{B}}(\theta_{\mathrm{T}}, \theta_{\mathrm{R}})\mathbf{X} + \mathbf{Z}_{\mathrm{R}} \tag{7}$$

where each element $y_{\mathrm{R}i,j}$ is the j-th fast-time snapshot received at the i-th antenna, $\mathbf{Z}_{\mathrm{R}}$ is the AWGN matrix, with covariance $\frac{1}{L}\mathbb{E}\{\mathbf{Z}_{\mathrm{R}}^{\mathsf{H}}\mathbf{Z}_{\mathrm{R}}\} = \sigma_{\mathrm{R}}^2\mathbf{I}_L$, and $\mathbf{A}_{\mathrm{B}}(\theta_{\mathrm{T}}, \theta_{\mathrm{R}}) \in \mathbb{C}^{N_{\mathrm{R}}\times N_{\mathrm{T}}}$ is a matrix depending on the steering vectors $\mathbf{a}(\theta_{\mathrm{T}}) \in \mathbb{C}^{N_{\mathrm{T}}\times 1}$ at the Tx and $\mathbf{b}(\theta_{\mathrm{R}}) \in \mathbb{C}^{N_{\mathrm{R}}\times 1}$ at the Rx [48], i.e.,

$$\mathbf{A}_{\mathrm{B}}(\theta_{\mathrm{T}}, \theta_{\mathrm{R}}) \triangleq \mathbf{b}(\theta_{\mathrm{R}})\mathbf{a}^{\mathsf{H}}(\theta_{\mathrm{T}})\,. \tag{8}$$

For uniform linear arrays (ULAs) with half-wavelength inter-element spacing, the steering vectors are

$$\mathbf{a}(\theta_{\mathrm{T}}) = \left[e^{-j\frac{N_{\mathrm{T}}-1}{2}\pi\sin\theta_{\mathrm{T}}}, e^{-j\frac{N_{\mathrm{T}}-3}{2}\pi\sin\theta_{\mathrm{T}}}, \ldots, e^{j\frac{N_{\mathrm{T}}-1}{2}\pi\sin\theta_{\mathrm{T}}}\right]^{\mathsf{T}}$$

$$\mathbf{b}(\theta_{\mathrm{R}}) = \left[e^{-j\frac{N_{\mathrm{R}}-1}{2}\pi\sin\theta_{\mathrm{R}}}, e^{-j\frac{N_{\mathrm{R}}-3}{2}\pi\sin\theta_{\mathrm{R}}}, \ldots, e^{j\frac{N_{\mathrm{R}}-1}{2}\pi\sin\theta_{\mathrm{R}}}\right]^{\mathsf{T}} \tag{9}$$

from which it can be readily noticed that

$$\mathbf{a}^{\mathsf{H}}(\theta_{\mathrm{T}})\mathbf{a}(\theta_{\mathrm{T}}) = N_{\mathrm{T}}, \quad \mathbf{b}^{\mathsf{H}}(\theta_{\mathrm{R}})\mathbf{b}(\theta_{\mathrm{R}}) = N_{\mathrm{R}}, \ \forall\theta_{\mathrm{T}}, \theta_{\mathrm{R}}\,. \tag{10}$$

Moreover, the derivatives $\dot{\mathbf{a}}(\theta_{\mathrm{T}}) \triangleq \frac{d\mathbf{a}(\theta_{\mathrm{T}})}{d\theta_{\mathrm{T}}}$ and $\dot{\mathbf{b}}(\theta_{\mathrm{R}}) \triangleq \frac{d\mathbf{b}(\theta_{\mathrm{R}})}{d\theta_{\mathrm{R}}}$ result in

$$\begin{aligned}
\dot{\mathbf{a}}(\theta_{\mathrm{T}}) = &\left[-ja_1\frac{N_{\mathrm{T}}-1}{2}\pi\cos\theta_{\mathrm{T}}, -ja_2\frac{N_{\mathrm{T}}-3}{2}\pi\cos\theta_{\mathrm{T}}, \ldots,\right.\\
&\left. ja_{N_{\mathrm{T}}}\frac{N_{\mathrm{T}}-1}{2}\pi\cos\theta_{\mathrm{T}}\right]^{\mathsf{T}}\\
\dot{\mathbf{b}}(\theta_{\mathrm{R}}) = &\left[-jb_1\frac{N_{\mathrm{R}}-1}{2}\pi\cos\theta_{\mathrm{R}}, -jb_2\frac{N_{\mathrm{R}}-3}{2}\pi\cos\theta_{\mathrm{R}}, \ldots,\right.\\
&\left. jb_{N_{\mathrm{R}}}\frac{N_{\mathrm{R}}-1}{2}\pi\cos\theta_{\mathrm{R}}\right]^{\mathsf{T}}
\end{aligned} \tag{11}$$

where a_i and b_i are the i-th elements of $\mathbf{a}(\theta_{\mathrm{T}})$ and $\mathbf{b}(\theta_{\mathrm{R}})$, respectively. It is easy to verify the following orthogonality property between steering vectors and their derivatives [48]:

$$\dot{\mathbf{a}}^{\mathsf{H}}(\theta_{\mathrm{T}})\mathbf{a}(\theta_{\mathrm{T}}) = \dot{\mathbf{b}}^{\mathsf{H}}(\theta_{\mathrm{R}})\mathbf{b}(\theta_{\mathrm{R}}) = 0, \ \forall\theta_{\mathrm{T}}, \theta_{\mathrm{R}}\,. \tag{12}$$

The log-likelihood of the received echo signal (7) can thus be derived as [66]

$$\begin{aligned}
\ln f_{\mathbf{Y}_{\mathrm{R}}}(\mathbf{Y}_{\mathrm{R}}; \theta_{\mathrm{T}}, \theta_{\mathrm{R}}) = &-N_{\mathrm{R}}L\ln(\pi\sigma_{\mathrm{R}}^2)\\
&- \frac{1}{\sigma_{\mathrm{R}}^2}\sum_{j=1}^{L}\Big(\|\mathbf{y}_j\|^2 - 2\Re\left\{\alpha\mathbf{y}_j^{\mathsf{H}}\mathbf{A}_{\mathrm{B}}(\theta_{\mathrm{T}}, \theta_{\mathrm{R}})\mathbf{x}_j\right\}\\
&+|\alpha|^2\mathbf{x}_j^{\mathsf{H}}\mathbf{A}_{\mathrm{B}}(\theta_{\mathrm{T}}, \theta_{\mathrm{R}})^{\mathsf{H}}\mathbf{A}_{\mathrm{B}}(\theta_{\mathrm{T}}, \theta_{\mathrm{R}})\mathbf{x}_j\Big)\,.
\end{aligned} \tag{13}$$

Now, since our goal is to derive the Fisher information matrix (FIM), we take the expectation of the negative log-likelihood (13), which after some calculations, and considering that the transmitted symbols are zero-mean (i.e., $\mathbb{E}\{\mathbf{x}_j\} = \mathbf{0}_{N_{\mathrm{T}}}$), leads to

$$\begin{aligned}
\mathcal{L}(\theta_{\mathrm{T}}, \theta_{\mathrm{R}}) &= -\mathbb{E}\left\{\ln f_{\mathbf{Y}_{\mathrm{R}}}(\mathbf{Y}_{\mathrm{R}}; \theta_{\mathrm{T}}, \theta_{\mathrm{R}})\right\}\\
&\propto \frac{|\alpha|^2}{\sigma_{\mathrm{R}}^2}\sum_{j=1}^{L}\mathbb{E}\left\{\mathbf{x}_j^{\mathsf{H}}\mathbf{A}_{\mathrm{B}}(\theta_{\mathrm{T}}, \theta_{\mathrm{R}})^{\mathsf{H}}\mathbf{A}_{\mathrm{B}}(\theta_{\mathrm{T}}, \theta_{\mathrm{R}})\mathbf{x}_j\right\}
\end{aligned} \tag{14}$$

where we dropped all the terms that do not depend on the parameters θ_{T} and θ_{R}. Now, recalling the properties of the trace operator we get

$$\begin{aligned}
\mathcal{L}(\theta_{\mathrm{T}}, \theta_{\mathrm{R}}) &\propto \frac{|\alpha|^2}{\sigma_{\mathrm{R}}^2}\sum_{j=1}^{L}\mathbb{E}\left\{\mathrm{tr}\left(\mathbf{A}_{\mathrm{B}}(\theta_{\mathrm{T}}, \theta_{\mathrm{R}})\mathbf{x}_j\mathbf{x}_j^{\mathsf{H}}\mathbf{A}_{\mathrm{B}}(\theta_{\mathrm{T}}, \theta_{\mathrm{R}})^{\mathsf{H}}\right)\right\}\\
&= \frac{L|\alpha|^2}{\sigma_{\mathrm{R}}^2}\mathrm{tr}\left(\mathbf{A}_{\mathrm{B}}(\theta_{\mathrm{T}}, \theta_{\mathrm{R}})\mathbf{R}_{\mathrm{X}}\mathbf{A}_{\mathrm{B}}^{\mathsf{H}}(\theta_{\mathrm{T}}, \theta_{\mathrm{R}})\right)\,.
\end{aligned} \tag{15}$$

Note that the covariance matrix $\mathbf{R}_{\mathrm{X}}$ in (15) is directly related to the beamforming vector $\mathbf{w}$ at the Tx via (2). Hence, such

[2]Typically, radar systems operate in LoS conditions due to the significant impact of path loss, as described by the radar equation, which severely limits detection and localization performance in non-line-of-sight scenarios.

a beamforming vector impacts both the communication functionality and the sensing one; therefore, $\mathbf{w}$ must be designed to achieve the desired communication/sensing trade-off.

In this work, we focus on target tracking scenarios, particularly those where the target is stationary or moving slowly. Under these conditions, the estimated or predicted positions evolve gradually, making the design of the beamforming pattern feasible.[3]

C. Bistatic Sensing Geometry

Without loss of generality, we can set the origin of the Cartesian axes on the center of the receiving array, such that the target position can be expressed as

$$x = d_{\mathrm{R}} \sin\theta_{\mathrm{R}} \tag{16a}$$

$$y = d_{\mathrm{R}} \cos\theta_{\mathrm{R}} \tag{16b}$$

where θ_{R} is anti-clockwise oriented, while the x-axis is oriented from right to left (see Fig. 1).

Consider the triangle with vertices in the target and in the Tx and the Rx. Once the baseline l is known, it is sufficient to know two out of the four following quantities to determine the target position: $d_{\mathrm{T}}, d_{\mathrm{R}}, \theta_{\mathrm{T}}, \theta_{\mathrm{R}}$. In the following, we choose to estimate the two angles θ_{T} and θ_{R}.[4]

Thus, to find the relationship between target position and the two angles, we can start writing the equations of the two lines shown in Fig. 1 that respectively pass through the target and the origin (0,0), and the target and the point $(l, 0)$, i.e.,

$$y = x \tan\left(\frac{\pi}{2} - \theta_{\mathrm{R}}\right) \tag{17}$$

$$y = (x - l) \tan\left(\theta_{\mathrm{T}} - \frac{\pi}{2}\right) \tag{18}$$

from which the x-coordinate of the intersection is obtained by equating (17) and (18)

$$x = \frac{l \tan\left(\theta_{\mathrm{T}} - \frac{\pi}{2}\right)}{\tan\left(\theta_{\mathrm{T}} - \frac{\pi}{2}\right) - \tan\left(\frac{\pi}{2} - \theta_{\mathrm{R}}\right)}. \tag{19}$$

Now, remembering the following trigonometric identity $\tan(\varphi - \frac{\pi}{2}) = -\tan(\frac{\pi}{2} - \varphi) = -\cot\varphi$, the expression (19) simplifies into

$$x = \frac{l}{1 + \cot\theta_{\mathrm{R}} \tan\theta_{\mathrm{T}}}. \tag{20}$$

Then, the y-coordinate of the target is obtained by substituting (20) in (17), from which

$$y = \frac{l}{\tan\theta_{\mathrm{R}} + \tan\theta_{\mathrm{T}}}. \tag{21}$$

Accordingly, we can define the following change of coordinates: $\Omega : (\theta_{\mathrm{T}}, \theta_{\mathrm{R}}) \to (x, y) = \Omega(\theta_{\mathrm{T}}, \theta_{\mathrm{R}})$ where

$$x = \phi(\theta_{\mathrm{T}}, \theta_{\mathrm{R}}) \triangleq \frac{l}{1 + \cot\theta_{\mathrm{R}} \tan\theta_{\mathrm{T}}} \tag{22a}$$

$$y = \psi(\theta_{\mathrm{T}}, \theta_{\mathrm{R}}) \triangleq \frac{l}{\tan\theta_{\mathrm{R}} + \tan\theta_{\mathrm{T}}}. \tag{22b}$$

[3]This assumption aligns with that adopted in [9] for the monostatic scenario, where $\mathbf{w}$ is optimized for a direction of interest in which a potential target may be located.

[4]Another possible solution is to estimate θ_{R} and $d_{\mathrm{T}} + d_{\mathrm{R}}$, the last one through the time difference of arrival between the Tx-Rx path and the Tx-target-Rx path.

Now, the target position is expressed in terms of the two angles $\theta_{\mathrm{R}}, \theta_{\mathrm{T}}$ to be estimated.

Remark 1: Note that when $y = 0$, i.e., the target is on the baseline, $\cot\theta_{\mathrm{R}} = 0$ and $\tan\theta_{\mathrm{T}} \to \infty$, therefore an indeterminate form arises for the x-coordinate in (22). Consequently, as is common in bistatic configurations, target localization is not feasible in this specific situation.

Remark 2: Note also that (22) are valid for $0 \le \theta_{\mathrm{T}} \le 2\pi$ and $0 \le \theta_{\mathrm{R}} \le 2\pi$. However, when using ULA antennas, care must be taken due to potential angle ambiguity. For instance, with ULAs oriented as in Fig. 1, it is advisable to restrict both θ_{T} and θ_{R} to $[-\pi/2, \pi/2]$ to avoid ambiguities in AoA and AoD estimation, unless specific information is available to resolve this ambiguity.

III. Communication vs Sensing Trade-Off

A. Fisher Information Matrix for Bistatic Sensing

Let us define

$$\dot{\mathbf{A}}_{\mathrm{T}}(\theta_{\mathrm{T}}, \theta_{\mathrm{R}}) \triangleq \frac{\partial \mathbf{A}_{\mathrm{B}}(\theta_{\mathrm{T}}, \theta_{\mathrm{R}})}{\partial \theta_{\mathrm{T}}} = \mathbf{b}(\theta_{\mathrm{R}}) \dot{\mathbf{a}}^{\mathsf{H}}(\theta_{\mathrm{T}}) \tag{23a}$$

$$\dot{\mathbf{A}}_{\mathrm{R}}(\theta_{\mathrm{T}}, \theta_{\mathrm{R}}) \triangleq \frac{\partial \mathbf{A}_{\mathrm{B}}(\theta_{\mathrm{T}}, \theta_{\mathrm{R}})}{\partial \theta_{\mathrm{R}}} = \dot{\mathbf{b}}(\theta_{\mathrm{R}}) \mathbf{a}^{\mathsf{H}}(\theta_{\mathrm{T}}). \tag{23b}$$

By observing (15), one can recognize that the FIM coefficients can be computed by following a procedure similar to that adopted in [48], obtaining:

$$J_{\theta_{\mathrm{T}},\theta_{\mathrm{T}}} = \frac{2L}{\sigma_{\mathrm{R}}^2} |\alpha|^2 \mathrm{tr}\left(\dot{\mathbf{A}}_{\mathrm{T}}(\theta_{\mathrm{T}}, \theta_{\mathrm{R}}) \mathbf{R}_{\mathrm{X}} \dot{\mathbf{A}}_{\mathrm{T}}^{\mathsf{H}}(\theta_{\mathrm{T}}, \theta_{\mathrm{R}})\right) \tag{24a}$$

$$J_{\theta_{\mathrm{T}},\theta_{\mathrm{R}}} = \frac{2L}{\sigma_{\mathrm{R}}^2} |\alpha|^2 \mathrm{tr}\left(\dot{\mathbf{A}}_{\mathrm{T}}(\theta_{\mathrm{T}}, \theta_{\mathrm{R}}) \mathbf{R}_{\mathrm{X}} \dot{\mathbf{A}}_{\mathrm{R}}^{\mathsf{H}}(\theta_{\mathrm{T}}, \theta_{\mathrm{R}})\right) = 0 \tag{24b}$$

$$J_{\theta_{\mathrm{R}},\theta_{\mathrm{T}}} = \frac{2L}{\sigma_{\mathrm{R}}^2} |\alpha|^2 \mathrm{tr}\left(\dot{\mathbf{A}}_{\mathrm{R}}(\theta_{\mathrm{T}}, \theta_{\mathrm{R}}) \mathbf{R}_{\mathrm{X}} \dot{\mathbf{A}}_{\mathrm{T}}^{\mathsf{H}}(\theta_{\mathrm{T}}, \theta_{\mathrm{R}})\right) = 0 \tag{24c}$$

$$J_{\theta_{\mathrm{R}},\theta_{\mathrm{R}}} = \frac{2L}{\sigma_{\mathrm{R}}^2} |\alpha|^2 \mathrm{tr}\left(\dot{\mathbf{A}}_{\mathrm{R}}(\theta_{\mathrm{T}}, \theta_{\mathrm{R}}) \mathbf{R}_{\mathrm{X}} \dot{\mathbf{A}}_{\mathrm{R}}^{\mathsf{H}}(\theta_{\mathrm{T}}, \theta_{\mathrm{R}})\right). \tag{24d}$$

Thus, the FIM results in the 2×2 diagonal matrix:

$$\mathcal{I}(\theta_{\mathrm{T}}, \theta_{\mathrm{R}}) = \begin{bmatrix} J_{\theta_{\mathrm{T}},\theta_{\mathrm{T}}} & 0 \\ 0 & J_{\theta_{\mathrm{R}},\theta_{\mathrm{R}}} \end{bmatrix}. \tag{25}$$

B. CRB on the AoA and AoD Estimation

The CRB on the AoA and AoD estimation error can be computed by inverting the FIM (25):

$$\mathcal{I}^{-1}(\theta_{\mathrm{T}}, \theta_{\mathrm{R}}) = \begin{bmatrix} \frac{1}{J_{\theta_{\mathrm{T}},\theta_{\mathrm{T}}}} & 0 \\ 0 & \frac{1}{J_{\theta_{\mathrm{R}},\theta_{\mathrm{R}}}} \end{bmatrix} \tag{26}$$

where $J_{\theta_{\mathrm{T}},\theta_{\mathrm{T}}}$ and $J_{\theta_{\mathrm{R}},\theta_{\mathrm{R}}}$ are defined by (24). Hence, the CRBs on the angles of arrival and departure are given by:

$$\mathrm{CRB}_{\theta_{\mathrm{T}}}(\theta_{\mathrm{T}}, \theta_{\mathrm{R}}) = \frac{\sigma_{\mathrm{R}}^2}{2L\, |\alpha|^2 \mathrm{tr}\left(\dot{\mathbf{A}}_{\mathrm{T}}(\theta_{\mathrm{T}}, \theta_{\mathrm{R}}) \mathbf{R}_{\mathrm{X}} \dot{\mathbf{A}}_{\mathrm{T}}^{\mathsf{H}}(\theta_{\mathrm{T}}, \theta_{\mathrm{R}})\right)} \tag{27a}$$

$$\mathrm{CRB}_{\theta_R}(\theta_T,\theta_R)=\frac{\sigma_R^2}{2L\,|\alpha|^2\mathrm{tr}\left(\dot{\mathbf{A}}_R(\theta_T,\theta_R)\mathbf{R}_X\dot{\mathbf{A}}_R^H(\theta_T,\theta_R)\right)}. \tag{27b}$$

C. CRB on the MSE of the Position Estimate

Let us denote with $\mathbf{J}_\Omega$ the Jacobian of the transformation $\Omega:(\theta_T,\theta_R)\rightarrow(x,y)=\Omega(\theta_T,\theta_R)$ defined by (22)

$$\mathbf{J}_\Omega\triangleq\begin{bmatrix}\frac{\partial\phi}{\partial\theta_T} & \frac{\partial\phi}{\partial\theta_R}\\ \frac{\partial\psi}{\partial\theta_T} & \frac{\partial\psi}{\partial\theta_R}\end{bmatrix} \tag{28}$$

whose elements are

$$\frac{\partial\phi}{\partial\theta_T}=-\frac{l\,\tan\theta_R}{\cos^2\theta_T(\tan\theta_R+\tan\theta_T)^2} \tag{29a}$$

$$\frac{\partial\phi}{\partial\theta_R}=\frac{l\,\tan\theta_T}{\cos^2\theta_R(\tan\theta_R+\tan\theta_T)^2} \tag{29b}$$

$$\frac{\partial\psi}{\partial\theta_T}=-\frac{l}{\cos^2\theta_T(\tan\theta_R+\tan\theta_T)^2} \tag{29c}$$

$$\frac{\partial\psi}{\partial\theta_R}=-\frac{l}{\cos^2\theta_R(\tan\theta_R+\tan\theta_T)^2}. \tag{29d}$$

By defining the inverse transformation $\Omega^{-1}:(x,y)\rightarrow(\theta_T,\theta_R)=\Omega^{-1}(x,y)$, it is known that its Jacobian is

$$\mathbf{J}_{\Omega^{-1}}=\mathbf{J}_\Omega^{-1} \tag{30}$$

from which the FIM with respect to the new coordinates, $\mathcal{I}(x,y)$, can be retrieved from

$$\mathcal{I}(x,y)=\mathbf{J}_{\Omega^{-1}}^{\mathsf{T}}\mathcal{I}(\theta_T,\theta_R)\mathbf{J}_{\Omega^{-1}} \tag{31}$$

and, thanks to (26) and (30), its inverse as

$$\begin{aligned}\mathcal{I}^{-1}(x,y)&=\mathbf{J}_\Omega\,\mathcal{I}^{-1}(\theta_T,\theta_R)\mathbf{J}_\Omega^{\mathsf{T}}\\&=\begin{bmatrix}\frac{\partial\phi}{\partial\theta_T} & \frac{\partial\phi}{\partial\theta_R}\\ \frac{\partial\psi}{\partial\theta_T} & \frac{\partial\psi}{\partial\theta_R}\end{bmatrix}\begin{bmatrix}\frac{1}{J_{\theta_T,\theta_T}} & 0\\ 0 & \frac{1}{J_{\theta_R,\theta_R}}\end{bmatrix}\begin{bmatrix}\frac{\partial\phi}{\partial\theta_T} & \frac{\partial\psi}{\partial\theta_T}\\ \frac{\partial\phi}{\partial\theta_R} & \frac{\partial\psi}{\partial\theta_R}\end{bmatrix}.\end{aligned} \tag{32}$$

Then, starting from (32), it follows that the CRB on target localization error is

$$\begin{aligned}\mathrm{CRB}(x,y)&=\mathrm{tr}\left(\mathcal{I}^{-1}(x,y)\right)=\mathrm{tr}\left(\mathbf{J}_\Omega\,\mathcal{I}^{-1}(\theta_T,\theta_R)\mathbf{J}_\Omega^{\mathsf{T}}\right)\\&=\mathrm{tr}\left(\mathbf{J}_\Omega^{\mathsf{T}}\mathbf{J}_\Omega\,\mathcal{I}^{-1}(\theta_T,\theta_R)\right)\end{aligned} \tag{33}$$

where

$$\mathbf{J}_\Omega^{\mathsf{T}}\mathbf{J}_\Omega=\mathbf{G}=\begin{bmatrix}g_{TT} & g_{TR}\\ g_{RT} & g_{RR}\end{bmatrix}=\begin{bmatrix}\frac{\partial\phi}{\partial\theta_T} & \frac{\partial\psi}{\partial\theta_T}\\ \frac{\partial\phi}{\partial\theta_R} & \frac{\partial\psi}{\partial\theta_R}\end{bmatrix}\begin{bmatrix}\frac{\partial\phi}{\partial\theta_T} & \frac{\partial\phi}{\partial\theta_R}\\ \frac{\partial\psi}{\partial\theta_T} & \frac{\partial\psi}{\partial\theta_R}\end{bmatrix}. \tag{34}$$

By substituting (26) in (33) the CRB expression can be further simplified as

$$\mathrm{CRB}(x,y)=\frac{g_{TT}}{J_{\theta_T,\theta_T}}+\frac{g_{RR}}{J_{\theta_R,\theta_R}} \tag{35}$$

where g_{TT} and g_{RR}, are computed starting from (29) and (34), as follows:

$$g_{TT}=\left(\frac{\partial\phi}{\partial\theta_T}\right)^2+\left(\frac{\partial\psi}{\partial\theta_T}\right)^2=\frac{l^2\,(1+\tan^2\theta_R)}{\cos^4\theta_T(\tan\theta_R+\tan\theta_T)^4} \tag{36a}$$

$$g_{RR}=\left(\frac{\partial\phi}{\partial\theta_R}\right)^2+\left(\frac{\partial\psi}{\partial\theta_R}\right)^2=\frac{l^2\,(1+\tan^2\theta_T)}{\cos^4\theta_R(\tan\theta_R+\tan\theta_T)^4}. \tag{36b}$$

Note that, from (22), we obtain:

$$\theta_R=\arctan\left(\frac{x}{y}\right),\quad\theta_T=\arctan\left(\frac{l-x}{y}\right) \tag{37}$$

that allows to write (36a) and (36b) and the CRB as a function of x and y.[5]

By using (24) in (35), the CRB of target position estimation can be written as

$$\begin{aligned}\mathrm{CRB}(x,y)=\frac{\sigma_R^2}{2L|\alpha|^2}\Bigg[&\frac{g_{TT}}{\mathrm{tr}\left(\dot{\mathbf{A}}_T(\theta_T,\theta_R)\mathbf{R}_X\dot{\mathbf{A}}_T^H(\theta_T,\theta_R)\right)}\\&+\frac{g_{RR}}{\mathrm{tr}\left(\dot{\mathbf{A}}_R(\theta_T,\theta_R)\mathbf{R}_X\dot{\mathbf{A}}_R^H(\theta_T,\theta_R)\right)}\Bigg].\end{aligned} \tag{38}$$

D. CRB Coefficients g_{TT} and g_{RR}

In Fig. 2(a), we plot the coefficient g_{TT} in the CRB expression (35), normalized to l^2 and expressed in logarithmic units, as a function of the target position (x,y). It can be noticed that the coefficient assumes high values (around 20 dB) along the baseline and low values (around -20 dB) approximately around the position $(l,0)$. The symmetry with respect to the x-axis can also be noticed.

In Fig. 2(b), instead, the g_{RR} coefficient in the CRB expression (35), normalized to l^2 and expressed in logarithmic units, is plotted as a function of the target position (x,y). We can notice that the coefficient assumes high values (around 20 dB) along the baseline and low values (around -20 dB) in (0,0) (at the Rx). To understand how the two coefficients impact the CRB it is interesting to compare them. In Fig. 2(c), the ratio g_{TT}/g_{RR} it deciBel is depicted, in order to partition the whole plane in three zones, where: *i)* $g_{TT}\geq g_{RR}$, *ii)* $g_{TT}\approx g_{RR}$, and *iii)* $g_{TT}\leq g_{RR}$. For each one of these zones, the *suboptimal method 1* will be applied according to Section IV-D1. These coefficients are also needed for the optimal solution as it will be shown in the next section.

IV. JSC Optimization for Bistatic Sensing

A. Problem Formulation

For the point target scenario with fixed target position (x,y), the beamforming optimization problem under communication user's SINR and power budget constraints can be written as:

$$\begin{aligned}\mathbf{W}_{\mathrm{opt}}=\;&\arg\min_{\mathbf{W}_{\mathrm{DF}}}\mathrm{CRB}(x,y)\\ \text{s.t.}\;\;&\gamma_k\geq\Gamma_k,\;\forall k\\&\|\mathbf{W}_{\mathrm{DF}}\|_F^2\leq P_T.\end{aligned} \tag{39}$$

[5]Note that these coefficients depend only on the position of the target and not on the beamforming vector, which instead affects J_{θ_T,θ_T} and J_{θ_R,θ_R} in (35).

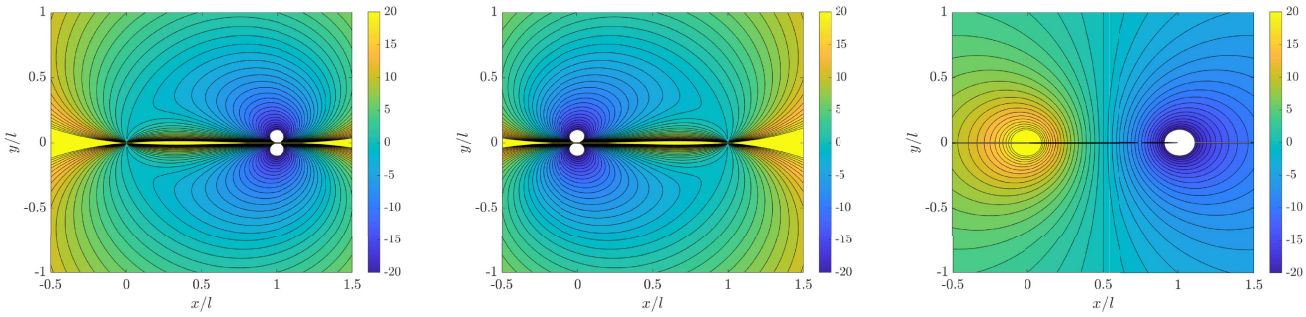

Fig. 2. Normalized coefficients: (a) g_{TT}/l^2 [dB], (b) g_{RR}/l^2 [dB], and (c) $g_{\mathrm{TT}}/g_{\mathrm{RR}}$ [dB].

B. Optimization for the Multiuser Case

By applying the Schur component condition as in [53] it can be proved that minimizing $\mathrm{CRB}(x,y)$ is equivalent to the following SDP:

$$\begin{aligned}\min_{\mathbf{R}_{\mathrm{X}}\succeq 0, t_{\mathrm{T}}, t_{\mathrm{R}}} \quad & \frac{\sigma_{\mathrm{R}}^2}{2L|\alpha|^2}\left(\frac{g_{\mathrm{TT}}}{t_{\mathrm{T}}}+\frac{g_{\mathrm{RR}}}{t_{\mathrm{R}}}\right)\\ \text{s.t.} \quad & \begin{bmatrix} t_{\mathrm{T}} & 0\\ 0 & \mathrm{tr}\left(\dot{\mathbf{A}}_{\mathrm{T}}^{\mathsf{H}}(\theta_{\mathrm{T}},\theta_{\mathrm{R}})\dot{\mathbf{A}}_{\mathrm{T}}(\theta_{\mathrm{T}},\theta_{\mathrm{R}})\mathbf{R}_{\mathrm{X}}\right)\end{bmatrix}\succeq 0\\ & \begin{bmatrix} t_{\mathrm{R}} & 0\\ 0 & \mathrm{tr}\left(\dot{\mathbf{A}}_{\mathrm{R}}^{\mathsf{H}}(\theta_{\mathrm{T}},\theta_{\mathrm{R}})\dot{\mathbf{A}}_{\mathrm{R}}(\theta_{\mathrm{T}},\theta_{\mathrm{R}})\mathbf{R}_{\mathrm{X}}\right)\end{bmatrix}\succeq 0\,.\end{aligned} \tag{40}$$

Thus, by noticing that $\mathbf{R}_{\mathrm{X}}=\mathbf{W}_{\mathrm{DF}}\mathbf{W}_{\mathrm{DF}}^{\mathsf{H}}=\sum_{k=1}^{K}\mathbf{w}_k\mathbf{w}_k^{\mathsf{H}}$, the problem (39) becomes:

$$\begin{aligned}\min_{\{\mathbf{w}_k\}_{k=1}^K\mathbf{R}_{\mathrm{X}}, t_{\mathrm{T}}, t_{\mathrm{R}}} \quad & \frac{\sigma_{\mathrm{R}}^2}{2L|\alpha|^2}\left(\frac{g_{\mathrm{TT}}}{t_{\mathrm{T}}}+\frac{g_{\mathrm{RR}}}{t_{\mathrm{R}}}\right)\\ \text{s.t.} \quad & \begin{bmatrix} t_{\mathrm{T}} & 0\\ 0 & \mathrm{tr}\left(\dot{\mathbf{A}}_{\mathrm{T}}^{\mathsf{H}}(\theta_{\mathrm{T}},\theta_{\mathrm{R}})\dot{\mathbf{A}}_{\mathrm{T}}(\theta_{\mathrm{T}},\theta_{\mathrm{R}})\mathbf{R}_{\mathrm{X}}\right)\end{bmatrix}\succeq 0\\ & \begin{bmatrix} t_{\mathrm{R}} & 0\\ 0 & \mathrm{tr}\left(\dot{\mathbf{A}}_{\mathrm{R}}^{\mathsf{H}}(\theta_{\mathrm{T}},\theta_{\mathrm{R}})\dot{\mathbf{A}}_{\mathrm{R}}(\theta_{\mathrm{T}},\theta_{\mathrm{R}})\mathbf{R}_{\mathrm{X}}\right)\end{bmatrix}\succeq 0\\ & \frac{|\mathbf{h}_k^{\mathsf{H}}\mathbf{w}_k|^2}{\sum_{\substack{i=1\\ i\neq k}}^{K}|\mathbf{h}_k^{\mathsf{H}}\mathbf{w}_i|^2+\sigma_{\mathrm{C}}^2}\geq\Gamma_k,\ \forall k\\ & \sum_{k=1}^{K}\mathrm{tr}\left(\mathbf{w}_k\mathbf{w}_k^{\mathsf{H}}\right)\leq P_{\mathrm{T}}\,,\quad \mathbf{R}_{\mathrm{X}}=\sum_{k=1}^{K}\mathbf{w}_k\mathbf{w}_k^{\mathsf{H}}\,.\end{aligned} \tag{41}$$

Let us define $\mathbf{Q}_k\triangleq\mathbf{h}_h\mathbf{h}_k^{\mathsf{H}}$ and $\mathbf{W}_k\triangleq\mathbf{w}_k\mathbf{w}_k^{\mathsf{H}}$. By using these quantities in the SINR constraints and by dropping the rank constraints on $\mathbf{W}_k$ for all k, the problem can be relaxed into a convex problem as follows:

$$\begin{aligned}\min_{\{\mathbf{W}_k\}_{k=1}^K, t_{\mathrm{T}}, t_{\mathrm{R}}} \quad & \frac{\sigma_{\mathrm{R}}^2}{2L|\alpha|^2}\left(\frac{g_{\mathrm{TT}}}{t_{\mathrm{T}}}+\frac{g_{\mathrm{RR}}}{t_{\mathrm{R}}}\right)\\ \text{s.t.} \quad & \begin{bmatrix} t_{\mathrm{T}} & 0\\ 0 & \mathrm{tr}\left(\dot{\mathbf{A}}_{\mathrm{T}}^{\mathsf{H}}(\theta_{\mathrm{T}},\theta_{\mathrm{R}})\dot{\mathbf{A}}_{\mathrm{T}}(\theta_{\mathrm{T}},\theta_{\mathrm{R}})\sum_{k=1}^{K}\mathbf{W}_k\right)\end{bmatrix}\succeq 0\\ & \begin{bmatrix} t_{\mathrm{R}} & 0\\ 0 & \mathrm{tr}\left(\dot{\mathbf{A}}_{\mathrm{R}}^{\mathsf{H}}(\theta_{\mathrm{T}},\theta_{\mathrm{R}})\dot{\mathbf{A}}_{\mathrm{R}}(\theta_{\mathrm{T}},\theta_{\mathrm{R}})\sum_{k=1}^{K}\mathbf{W}_k\right)\end{bmatrix}\succeq 0\\ & \mathrm{tr}\left(\mathbf{Q}_k\mathbf{W}_k\right)-\Gamma_k\sum_{\substack{k=1\\ i\neq k}}^{K}\mathrm{tr}\left(\mathbf{Q}_k\mathbf{W}_i\right)\geq\Gamma_k\sigma_{\mathrm{C}}^2,\ \forall k\\ & \sum_{k=1}^{K}\mathrm{tr}\left(\mathbf{W}_k\right)\leq P_{\mathrm{T}}\,,\quad \mathbf{W}_k\succeq 0\,.\end{aligned} \tag{42}$$

C. Optimization for the Single User Case

The case $K=1$ is of particular interest, as it leads to a simplified optimization procedure while still capturing the main features of the problem under consideration. Moreover, in practical scenarios such as multicarrier systems, multiple users can often be allocated orthogonally to avoid mutual interference. As a result, it is not uncommon for the trade-off to involve a single user and a target. Note that, for $K=1$, the dual function beamforming matrix $\mathbf{W}_{\mathrm{DF}}=(\mathbf{w}_1,\mathbf{w}_2,\ldots,\mathbf{w}_K)\in\mathbb{C}^{N_{\mathrm{T}}\times K}$ reduces to a vector $\mathbf{w}\in\mathbb{C}^{N_{\mathrm{T}}\times 1}$, where we skip the index $k=1$ for simplicity. Thus, the covariance matrix (2) reduces to $\mathbf{R}_{\mathrm{X}}=\mathbf{w}\mathbf{w}^{H}$, the power constraint (3) becomes simply:

$$\frac{1}{L}\sum_{i=1}^{N_{\mathrm{T}}}\sum_{j=1}^{L}|x_{ij}|^2=\frac{1}{L}\mathrm{tr}(\mathbf{X}\mathbf{X}^{\mathsf{H}})=\mathrm{tr}(\mathbf{w}\mathbf{w}^{\mathsf{H}})=\|\mathbf{w}\|^2\leq P_{\mathrm{T}} \tag{43}$$

and the SINR for the generic k-th user (5) reduce to the SNR of the single user:

$$\gamma=\frac{\|\mathbf{X}^{\mathsf{H}}\mathbf{h}\|^2}{L\sigma_{\mathrm{C}}^2}=\frac{\|\mathbf{w}^{\mathsf{H}}\mathbf{h}\|^2}{\sigma_{\mathrm{C}}^2}\,. \tag{44}$$

Moreover, by using (2), (8), (10), (12), and (23), as well as the circular property of the trace operator, (24) becomes:

$$\begin{aligned}J_{\theta_{\mathrm{T}},\theta_{\mathrm{T}}}&=\frac{2L}{\sigma_{\mathrm{R}}^2}|\alpha|^2\mathrm{tr}\left(\mathbf{b}(\theta_{\mathrm{R}})\dot{\mathbf{a}}^{\mathsf{H}}(\theta_{\mathrm{T}})\mathbf{w}\mathbf{w}^{\mathsf{H}}\dot{\mathbf{a}}(\theta_{\mathrm{T}})\mathbf{b}^{\mathsf{H}}(\theta_{\mathrm{R}})\right)\\ &=\frac{2L}{\sigma_{\mathrm{R}}^2}|\alpha|^2N_{\mathrm{R}}|\dot{\mathbf{a}}^{\mathsf{H}}(\theta_{\mathrm{T}})\mathbf{w}|^2 \qquad (45a)\\ J_{\theta_{\mathrm{T}},\theta_{\mathrm{R}}}&=\frac{2L}{\sigma_{\mathrm{R}}^2}|\alpha|^2\mathrm{tr}\left(\mathbf{b}(\theta_{\mathrm{R}})\dot{\mathbf{a}}^{\mathsf{H}}(\theta_{\mathrm{T}})\mathbf{w}\mathbf{w}^{\mathsf{H}}\mathbf{a}(\theta_{\mathrm{T}})\dot{\mathbf{b}}^{\mathsf{H}}(\theta_{\mathrm{R}})\right)=0 \qquad (45b)\\ J_{\theta_{\mathrm{R}},\theta_{\mathrm{T}}}&=J_{\theta_{\mathrm{T}},\theta_{\mathrm{R}}}^{*}=0 \qquad (45c)\end{aligned}$$

$$J_{\theta_R,\theta_R} = \frac{2L}{\sigma_R^2}|\alpha|^2 \mathrm{tr}\left(\dot{\mathbf{b}}(\theta_R)\mathbf{a}^H(\theta_T)\mathbf{w}\mathbf{w}^H\mathbf{a}(\theta_T)\dot{\mathbf{b}}^H(\theta_R)\right)$$
$$= \frac{2L}{\sigma_R^2}|\alpha|^2\|\dot{\mathbf{b}}(\theta_R)\|^2|\mathbf{a}^H(\theta_T)\mathbf{w}|^2\,. \quad (45d)$$

As a consequence, (27) reduces to:

$$\mathrm{CRB}_{\theta_T}(\theta_T,\theta_R) = \frac{\sigma_R^2}{2L\ |\alpha|^2 N_R|\dot{\mathbf{a}}^H(\theta_T)\mathbf{w}|^2} \quad (46a)$$

$$\mathrm{CRB}_{\theta_R}(\theta_T,\theta_R) = \frac{\sigma_R^2}{2L\ |\alpha|^2\|\dot{\mathbf{b}}(\theta_R)\|^2|\mathbf{a}^H(\theta_T)\mathbf{w}|^2}\,. \quad (46b)$$

Note that, due to the orthogonality between $\mathbf{a}$ and $\dot{\mathbf{a}}$, and the dependence of (46) on the projection of $\mathbf{w}$ onto them, the optimal weight vector is necessarily a compromise between the reduction of the two CRBs.

Finally, by using (45) in (35), the CRB of target position estimation can be written as

$$\mathrm{CRB}(x,y) = \frac{\sigma_R^2}{2L|\alpha|^2}\left(\frac{g_{TT}}{N_R\ |\dot{\mathbf{a}}^H(\theta_T)\mathbf{w}|^2} + \frac{g_{RR}}{\|\dot{\mathbf{b}}(\theta_R)\|^2|\mathbf{a}^H(\theta_T)\mathbf{w}|^2}\right). \quad (47)$$

Omitting, for the sake of clarity, the dependence on the angles, the CRB (47) can be further simplified to

$$\mathrm{CRB}(x,y) = \frac{\tilde{g}_T}{|\dot{\mathbf{a}}^H\mathbf{w}|^2} + \frac{\tilde{g}_R}{|\mathbf{a}^H\mathbf{w}|^2} \quad (48)$$

with

$$\tilde{g}_T \triangleq \frac{\sigma_R^2}{2L|\alpha|^2}\frac{g_{TT}}{N_R} \quad (49a)$$

$$\tilde{g}_R \triangleq \frac{\sigma_R^2}{2L|\alpha|^2}\frac{g_{RR}}{\|\dot{\mathbf{b}}(\theta_R)\|^2}\,. \quad (49b)$$

To optimize the beamforming at the Tx for JSC we need to solve the following problem:

$$\mathbf{w}_{\mathrm{opt}} = \arg\min_{\mathbf{w}} \mathrm{CRB}(x,y)$$
$$\text{s.t.}\quad |\mathbf{h}^H\mathbf{w}|^2 = \gamma\sigma_C^2$$
$$\|\mathbf{w}\|^2 = P_T. \quad (50)$$

Note that the problem makes sense only if $\gamma \le \|\mathsf{h}\|^2\ P_T/\sigma_C^2$. If this condition is not met, there is insufficient power to satisfy the communication SNR constraint, even if sensing is disregarded. In such a case, the only viable option is to allocate the entire amount of available power to the communication task. This can be achieved by choosing $\mathbf{w} = \frac{\mathbf{h}}{|\mathbf{h}|}\sqrt{P_T}$, thereby obtaining an actual SNR of $\|\mathbf{h}\|^2\ P_T/\sigma_C^2$.

Remark: Although the problem setting may appear similar to the monostatic case solved in [53], seeking the optimal beamforming in the bistatic case is significantly more complex due to a CRB composed of two terms (rather than just one) involving two orthogonal vectors, $\mathbf{a}$ and $\dot{\mathbf{a}}$, in the optimization problem. Therefore, the methodology to solve the problem is entirely new and must be sought in a three-dimensional subspace rather than a two-dimensional one, making this optimization not straightforward. Moreover, the approach presented in [53] finds the optimal beamforming only for AoA estimation, whereas we solve the more general problem for target position estimation.

In this section we develop a framework to obtain the analytical expression for the optimal JSC beamforming weights defined by the problem (50).

1) Optimal Weight Vector Evaluation: Let us start defining the following subspace:[6]

$$\mathcal{S} \triangleq \mathrm{Span}\{\mathbf{a},\dot{\mathbf{a}},\mathbf{h}\} \quad (51)$$

having the orthonormal basis:

$$\mathbf{u}_{\dot{\mathbf{a}}} \triangleq \frac{\dot{\mathbf{a}}}{\|\dot{\mathbf{a}}\|},\quad \mathbf{u}_{\mathbf{a}} \triangleq \frac{\mathbf{a}}{\|\mathbf{a}\|},\quad \mathbf{u}_t \triangleq \frac{\mathbf{v}}{\|\mathbf{v}\|} \quad (52)$$

where

$$\mathbf{v} \in \mathcal{S} : \mathbf{v}^H\mathbf{u}_{\mathbf{a}} = \mathbf{v}^H\mathbf{u}_{\dot{\mathbf{a}}} = 0\,. \quad (53)$$

Thus, because of the orthogonality between $\dot{\mathbf{a}}$ and $\mathbf{a}$, we can write

$$|\dot{\mathbf{a}}^H\mathbf{w}|^2 = |w_1|^2\|\dot{\mathbf{a}}\|^2 \quad (54a)$$

$$|\mathbf{a}^H\mathbf{w}|^2 = |w_2|^2\|\mathbf{a}\|^2 = N_T|w_2|^2 \quad (54b)$$

where by w_1 and w_2 we denote the components of $\mathbf{w}$ among $\mathbf{u}_{\dot{\mathbf{a}}}$ and $\mathbf{u}_{\mathbf{a}}$, respectively. By substituting (54) in (48), it results in:

$$\mathrm{CRB}(x,y) = \frac{\tilde{g}_T}{\|\dot{\mathbf{a}}\|^2|w_1|^2} + \frac{\tilde{g}_R}{N_T|w_2|^2}\,. \quad (55)$$

It is immediate from (55) that only the components of $\mathbf{w}$ among $\dot{\mathbf{a}}$ and $\mathbf{a}$ concur to the CRB. Besides, the SNR constraint (5) depends only on the components of $\mathbf{w}$ among $\mathbf{h}$. It follows from the power constraint that any component of $\mathbf{w}$ among directions not belonging to $\mathcal{S}$ would result in a waste of power that does not impact the CRB nor the SNR constraint. Thus, the optimal weight (50) has to belong to $\mathcal{S}$, i.e.,

$$\mathbf{w}_{\mathrm{opt}} = w_1\mathbf{u}_{\dot{\mathbf{a}}} + w_2\mathbf{u}_{\mathbf{a}} + w_3\mathbf{u}_t. \quad (56)$$

The problem (50) can be now restated as:

$$\mathbf{w}_{\mathrm{opt}} = \arg\min_{w_1,w_2,w_3} \frac{\tilde{g}_T}{\|\dot{\mathbf{a}}\|^2|w_1|^2} + \frac{\tilde{g}_R}{N_T|w_2|^2} \quad (57a)$$
$$\text{s.t.}\quad |w_1\mathbf{h}^H\mathbf{u}_{\dot{\mathbf{a}}} + w_2\mathbf{h}^H\mathbf{u}_{\mathbf{a}} + w_3\mathbf{h}^H\mathbf{u}_t|^2 = \gamma\sigma_C^2 \quad (57b)$$
$$|w_1|^2 + |w_2|^2 + |w_3|^2 = P_T. \quad (57c)$$

By following the Lagrange's multipliers method,[7] we write

$$\nabla\Bigg[\frac{\tilde{g}_T}{\|\dot{\mathbf{a}}\|^2|w_1|^2} + \frac{\tilde{g}_R}{N_T|w_2|^2} + \lambda\left(|w_1\mathbf{h}^H\mathbf{u}_{\dot{\mathbf{a}}} + w_2\mathbf{h}^H\mathbf{u}_{\mathbf{a}} + w_3\mathbf{h}^H\mathbf{u}_t|^2 - \gamma\sigma_C^2\right) + \mu\left(|w_1|^2 + |w_2|^2 + |w_3|^2 - P_T\right)\Bigg] = 0 \quad (58)$$

[6]We recall that the span of a set of vectors is defined as the set of all linear combinations that can be formed from those vectors.

[7]Note that the CRB function (57a) to be minimized is convex (except on the line $w_1 = 0$, $w_2 = 0$) and that the two constraints are represented by convex functions in $\mathbb{R}^3$.

where $\nabla[\cdot] \triangleq (\frac{\partial \cdot}{\partial w_1}, \frac{\partial \cdot}{\partial w_2}, \frac{\partial \cdot}{\partial w_3}, \frac{\partial \cdot}{\partial \lambda}, \frac{\partial \cdot}{\partial \mu})^{\mathsf{T}}$. By setting to zero the partial derivative with respect w_1, w_2, w_3, we obtain, after some algebra:

$$\mu w_1 = \frac{\tilde{g}_{\mathrm{T}}}{\|\dot{\mathbf{a}}\|^2|w_1|^4} w_1 - \lambda \left[w_1 |\mathbf{h}^{\mathsf{H}}\mathbf{u}_{\dot{\mathbf{a}}}|^2 + w_2 (\mathbf{h}^{\mathsf{H}}\mathbf{u}_{\mathbf{a}})(\mathbf{h}^{\mathsf{H}}\mathbf{u}_{\dot{\mathbf{a}}})^* + w_3 (\mathbf{h}^{\mathsf{H}}\mathbf{u}_{\mathrm{t}})(\mathbf{h}^{\mathsf{H}}\mathbf{u}_{\dot{\mathbf{a}}})^* \right] \quad (59a)$$

$$\mu w_2 = \frac{\tilde{g}_{\mathrm{R}}}{N_{\mathrm{T}}|w_2|^4} w_2 - \lambda \left[w_1 (\mathbf{h}^{\mathsf{H}}\mathbf{u}_{\dot{\mathbf{a}}})(\mathbf{h}^{\mathsf{H}}\mathbf{u}_{\mathbf{a}})^* + w_2 |\mathbf{h}^{\mathsf{H}}\mathbf{u}_{\mathbf{a}}|^2 + w_3 (\mathbf{h}^{\mathsf{H}}\mathbf{u}_{\mathrm{t}})(\mathbf{h}^{\mathsf{H}}\mathbf{u}_{\mathbf{a}})^* \right] \quad (59b)$$

$$\mu w_3 = -\lambda w_1 (\mathbf{h}^{\mathsf{H}}\mathbf{u}_{\dot{\mathbf{a}}})(\mathbf{h}^{\mathsf{H}}\mathbf{u}_{\mathrm{t}})^* - \lambda w_2 (\mathbf{h}^{\mathsf{H}}\mathbf{u}_{\mathbf{a}})(\mathbf{h}^{\mathsf{H}}\mathbf{u}_{\mathrm{t}})^* - \lambda w_3 |\mathbf{h}^{\mathsf{H}}\mathbf{u}_{\mathrm{t}}|^2 \quad (59c)$$

from which, we can re-write the last equation as

$$w_1 (\mathbf{h}^{\mathsf{H}}\mathbf{u}_{\dot{\mathbf{a}}}) + w_2 (\mathbf{h}^{\mathsf{H}}\mathbf{u}_{\mathbf{a}}) + w_3 (\mathbf{h}^{\mathsf{H}}\mathbf{u}_{\mathrm{t}}) = -\frac{\mu w_3}{\lambda (\mathbf{h}^{\mathsf{H}}\mathbf{u}_{\mathrm{t}})^*} \quad (60)$$

that, substituted in (59a), (59b), and (57b), provides

$$\frac{\tilde{g}_{\mathrm{T}}}{\|\dot{\mathbf{a}}\|^2|w_1|^4} w_1 + \mu w_3 \frac{(\mathbf{h}^{\mathsf{H}}\mathbf{u}_{\dot{\mathbf{a}}})^*}{(\mathbf{h}^{\mathsf{H}}\mathbf{u}_{\mathrm{t}})^*} = \mu w_1 \quad (61)$$

$$\frac{\tilde{g}_{\mathrm{R}}}{N_{\mathrm{T}}|w_2|^4} w_1 + \mu w_3 \frac{(\mathbf{h}^{\mathsf{H}}\mathbf{u}_{\mathbf{a}})^*}{(\mathbf{h}^{\mathsf{H}}\mathbf{u}_{\mathrm{t}})^*} = \mu w_2 \quad (62)$$

$$\frac{\mu^2 |w_3|^2}{\lambda^2 |\mathbf{h}^{\mathsf{H}}\mathbf{u}_{\mathrm{t}}|^2} = \gamma \sigma_{\mathrm{C}}^2. \quad (63)$$

Thus, (61) and (62) can be re-written as

$$\frac{\tilde{g}_{\mathrm{T}}}{\|\dot{\mathbf{a}}\|^2|w_1|^2 w_1^*} = \mu \left[w_1 - w_3 \frac{(\mathbf{h}^{\mathsf{H}}\mathbf{u}_{\dot{\mathbf{a}}})^*}{(\mathbf{h}^{\mathsf{H}}\mathbf{u}_{\mathrm{t}})^*} \right] \quad (64)$$

$$\frac{\tilde{g}_{\mathrm{R}}}{N_{\mathrm{T}}|w_2|^2 w_2^*} = \mu \left[w_2 - w_3 \frac{(\mathbf{h}^{\mathsf{H}}\mathbf{u}_{\mathbf{a}})^*}{(\mathbf{h}^{\mathsf{H}}\mathbf{u}_{\mathrm{t}})^*} \right] \quad (65)$$

and, by equaling μ in the two above equations, we get

$$\frac{\|\dot{\mathbf{a}}\|^2|w_1|^2 w_1^*}{\tilde{g}_{\mathrm{T}}} \left[w_1 - w_3 \frac{(\mathbf{h}^{\mathsf{H}}\mathbf{u}_{\dot{\mathbf{a}}})^*}{(\mathbf{h}^{\mathsf{H}}\mathbf{u}_{\mathrm{t}})^*} \right] = \frac{N_{\mathrm{T}}|w_2|^2 w_2^*}{\tilde{g}_{\mathrm{R}}} \left[w_2 - w_3 \frac{(\mathbf{h}^{\mathsf{H}}\mathbf{u}_{\mathbf{a}})^*}{(\mathbf{h}^{\mathsf{H}}\mathbf{u}_{\mathrm{t}})^*} \right]. \quad (66)$$

Lastly, by considering (66), the power constraint, and the SNR constraint, we obtain the following system of three equations with three unknowns:

$$\left(\frac{\|\dot{\mathbf{a}}\|^2|w_1|^4}{\tilde{g}_{\mathrm{T}}} - \frac{N_{\mathrm{T}}|w_2|^4}{\tilde{g}_{\mathrm{R}}} \right) (\mathbf{h}^{\mathsf{H}}\mathbf{u}_{\mathrm{t}})^* = \frac{\|\dot{\mathbf{a}}\|^2|w_1|^2 w_1^* w_3}{\tilde{g}_{\mathrm{T}}} (\mathbf{h}^{\mathsf{H}}\mathbf{u}_{\dot{\mathbf{a}}})^* - \frac{N_{\mathrm{T}}|w_2|^2 w_2^* w_3}{\tilde{g}_{\mathrm{R}}} (\mathbf{h}^{\mathsf{H}}\mathbf{u}_{\mathbf{a}})^* \quad (67a)$$

$$|w_1 \mathbf{h}^{\mathsf{H}}\mathbf{u}_{\dot{\mathbf{a}}} + w_2 \mathbf{h}^{\mathsf{H}}\mathbf{u}_{\mathbf{a}} + w_3 \mathbf{h}^{\mathsf{H}}\mathbf{u}_{\mathrm{t}}|^2 = \gamma \sigma_{\mathrm{C}}^2 \quad (67b)$$

$$|w_1|^2 + |w_2|^2 + |w_3|^2 = P_{\mathrm{T}} \quad (67c)$$

and from the first equation, we get

$$\mathbf{h}^{\mathsf{T}} \left[\left(\frac{\|\dot{\mathbf{a}}\|^2|w_1|^4}{\tilde{g}_{\mathrm{T}}} - \frac{N_{\mathrm{T}}|w_2|^4}{\tilde{g}_{\mathrm{R}}} \right) \mathbf{u}_{\mathrm{t}}^* \right] = \mathbf{h}^{\mathsf{T}} w_3 \left(\frac{\|\dot{\mathbf{a}}\|^2|w_1|^2 w_1^*}{\tilde{g}_{\mathrm{T}}} \mathbf{u}_{\dot{\mathbf{a}}}^* - \frac{N_{\mathrm{T}}|w_2|^2 w_2^*}{\tilde{g}_{\mathrm{R}}} \mathbf{u}_{\mathbf{a}}^* \right) \quad (68)$$

which leads to

$$w_3 = \frac{\left(\frac{\|\dot{\mathbf{a}}\|^2|w_1|^4}{\tilde{g}_{\mathrm{T}}} - \frac{N_{\mathrm{T}}|w_2|^4}{\tilde{g}_{\mathrm{R}}} \right) (\mathbf{h}^{\mathsf{H}}\mathbf{u}_{\mathrm{t}})^*}{\frac{\|\dot{\mathbf{a}}\|^2|w_1|^2 w_1^*}{\tilde{g}_{\mathrm{T}}} (\mathbf{h}^{\mathsf{H}}\mathbf{u}_{\dot{\mathbf{a}}})^* - \frac{N_{\mathrm{T}}|w_2|^2 w_2^*}{\tilde{g}_{\mathrm{R}}} (\mathbf{h}^{\mathsf{H}}\mathbf{u}_{\mathbf{a}})^*}. \quad (69)$$

Now, by observing (57), we note that the phases of w_1, w_2, and w_3 play a role in the SNR expression only and not in the CRB (57a). Thus, by using an argument similar to that adopted in [53], we have to choose these phases such that

$$\arg\{w_1\} + \arg\{\mathbf{h}^{\mathsf{H}}\mathbf{u}_{\dot{\mathbf{a}}}\} = \arg\{w_2\} + \arg\{\mathbf{h}^{\mathsf{H}}\mathbf{u}_{\mathbf{a}}\} = \arg\{w_3\} + \arg\{\mathbf{h}^{\mathsf{H}}\mathbf{u}_{\mathrm{t}}\} = \phi \quad (70)$$

with arbitrary ϕ. In other words, the phases of the addends in (57b) given the power constraint (57c), the sum will result in a lower SNR. Thus, (69) and (67b) become

$$|w_3| = \frac{\left(\frac{\|\dot{\mathbf{a}}\|^2|w_1|^4}{\tilde{g}_{\mathrm{T}}} - \frac{N_{\mathrm{T}}|w_2|^4}{\tilde{g}_{\mathrm{R}}} \right) |\mathbf{h}^{\mathsf{H}}\mathbf{u}_{\mathrm{t}}|}{\frac{\|\dot{\mathbf{a}}\|^2|w_1|^3}{\tilde{g}_{\mathrm{T}}} |\mathbf{h}^{\mathsf{H}}\mathbf{u}_{\dot{\mathbf{a}}}| - \frac{N_{\mathrm{T}}|w_2|^3}{\tilde{g}_{\mathrm{R}}} |\mathbf{h}^{\mathsf{H}}\mathbf{u}_{\mathbf{a}}|} \quad (71)$$

$$|w_1||\mathbf{h}^{\mathsf{H}}\mathbf{u}_{\dot{\mathbf{a}}}| + |w_2||\mathbf{h}^{\mathsf{H}}\mathbf{u}_{\mathbf{a}}| + |w_3||\mathbf{h}^{\mathsf{H}}\mathbf{u}_{\mathrm{t}}| = \sqrt{\gamma \sigma_{\mathrm{C}}^2}. \quad (72)$$

By using (69) in (67b) and (67c) we get:

$$|w_1||\mathbf{h}^{\mathsf{H}}\mathbf{u}_{\dot{\mathbf{a}}}| + |w_2||\mathbf{h}^{\mathsf{H}}\mathbf{u}_{\mathbf{a}}| + \frac{\left(\frac{\|\dot{\mathbf{a}}\|^2|w_1|^4}{\tilde{g}_{\mathrm{T}}} - \frac{N_{\mathrm{T}}|w_2|^4}{\tilde{g}_{\mathrm{R}}} \right) |\mathbf{h}^{\mathsf{H}}\mathbf{u}_{\mathrm{t}}|^2}{\frac{\|\dot{\mathbf{a}}\|^2|w_1|^3}{\tilde{g}_{\mathrm{T}}} |\mathbf{h}^{\mathsf{H}}\mathbf{u}_{\dot{\mathbf{a}}}| - \frac{N_{\mathrm{T}}|w_2|^3}{\tilde{g}_{\mathrm{R}}} |\mathbf{h}^{\mathsf{H}}\mathbf{u}_{\mathbf{a}}|} = \sqrt{\gamma \sigma_{\mathrm{C}}^2} \quad (73a)$$

$$|w_1|^2 + |w_2|^2 + \frac{\left(\frac{\|\dot{\mathbf{a}}\|^2|w_1|^4}{\tilde{g}_{\mathrm{T}}} - \frac{N_{\mathrm{T}}|w_2|^4}{\tilde{g}_{\mathrm{R}}} \right)^2 |\mathbf{h}^{\mathsf{H}}\mathbf{u}_{\mathrm{t}}|^2}{\left(\frac{\|\dot{\mathbf{a}}\|^2|w_1|^3}{\tilde{g}_{\mathrm{T}}} |\mathbf{h}^{\mathsf{H}}\mathbf{u}_{\dot{\mathbf{a}}}| - \frac{N_{\mathrm{T}}|w_2|^3}{\tilde{g}_{\mathrm{R}}} |\mathbf{h}^{\mathsf{H}}\mathbf{u}_{\mathbf{a}}| \right)^2} = P_{\mathrm{T}}. \quad (73b)$$

that can be re-arranged as:

$$\frac{\left(\frac{\|\dot{\mathbf{a}}\|^2|w_1|^4}{\tilde{g}_{\mathrm{T}}} - \frac{N_{\mathrm{T}}|w_2|^4}{\tilde{g}_{\mathrm{R}}} \right) |\mathbf{h}^{\mathsf{H}}\mathbf{u}_{\mathrm{t}}|}{\frac{\|\dot{\mathbf{a}}\|^2|w_1|^3}{\tilde{g}_{\mathrm{T}}} |\mathbf{h}^{\mathsf{H}}\mathbf{u}_{\dot{\mathbf{a}}}| - \frac{N_{\mathrm{T}}|w_2|^3}{\tilde{g}_{\mathrm{R}}} |\mathbf{h}^{\mathsf{H}}\mathbf{u}_{\mathbf{a}}|} = \frac{\sqrt{\gamma \sigma_{\mathrm{C}}^2} - |w_1||\mathbf{h}^{\mathsf{H}}\mathbf{u}_{\dot{\mathbf{a}}}| - |w_2||\mathbf{h}^{\mathsf{H}}\mathbf{u}_{\mathbf{a}}|}{|\mathbf{h}^{\mathsf{H}}\mathbf{u}_{\mathrm{t}}|} \quad (74a)$$

$$|w_1|^2 + |w_2|^2 + \frac{\left(\sqrt{\gamma \sigma_{\mathrm{C}}^2} - |w_1||\mathbf{h}^{\mathsf{H}}\mathbf{u}_{\dot{\mathbf{a}}}| - |w_2||\mathbf{h}^{\mathsf{H}}\mathbf{u}_{\mathbf{a}}| \right)^2}{|\mathbf{h}^{\mathsf{H}}\mathbf{u}_{\mathrm{t}}|^2} = P_{\mathrm{T}}. \quad (74b)$$

The (74a) can be rewritten as:

$$\left(\frac{\|\dot{\mathbf{a}}\|^2|w_1|^4}{\tilde{g}_{\mathrm{T}}} - \frac{N_{\mathrm{T}}|w_2|^4}{\tilde{g}_{\mathrm{R}}} \right) |\mathbf{h}^{\mathsf{H}}\mathbf{u}_{\mathrm{t}}|^2 = \sqrt{\gamma \sigma_{\mathrm{C}}^2} \frac{\|\dot{\mathbf{a}}\|^2|w_1|^3}{\tilde{g}_{\mathrm{T}}} |\mathbf{h}^{\mathsf{H}}\mathbf{u}_{\dot{\mathbf{a}}}| - \frac{\|\dot{\mathbf{a}}\|^2|w_1|^4}{\tilde{g}_{\mathrm{T}}} |\mathbf{h}^{\mathsf{H}}\mathbf{u}_{\dot{\mathbf{a}}}|^2$$

$$- \frac{\|\dot{\mathbf{a}}\|^2|w_1|^3|w_2|}{\tilde{g}_\mathrm{T}}|\mathbf{h}^\mathsf{H}\mathbf{u}_{\dot{\mathbf{a}}}||\mathbf{h}^\mathsf{H}\mathbf{u}_\mathbf{a}| - \sqrt{\gamma\sigma_\mathrm{C}^2}\frac{N_\mathrm{T}|w_2|^3}{\tilde{g}_\mathrm{R}}|\mathbf{h}^\mathsf{H}\mathbf{u}_\mathbf{a}|$$
$$+ \frac{N_\mathrm{T}|w_1||w_2|^3}{\tilde{g}_\mathrm{R}}|\mathbf{h}^\mathsf{H}\mathbf{u}_{\dot{\mathbf{a}}}||\mathbf{h}^\mathsf{H}\mathbf{u}_\mathbf{a}| + \frac{N_\mathrm{T}|w_2|^4}{\tilde{g}_\mathrm{R}}|\mathbf{h}^\mathsf{H}\mathbf{u}_\mathbf{a}|^2 \quad (75)$$

that is

$$\frac{\|\dot{\mathbf{a}}\|^2|w_1|^4}{\tilde{g}_\mathrm{T}}(|\mathbf{h}^\mathsf{H}\mathbf{u}_\mathrm{t}|^2 + |\mathbf{h}^\mathsf{H}\mathbf{u}_{\dot{\mathbf{a}}}|^2)$$
$$- \frac{N_\mathrm{T}|w_2|^4}{\tilde{g}_\mathrm{R}}(|\mathbf{h}^\mathsf{H}\mathbf{u}_\mathrm{t}|^2 + |\mathbf{h}^\mathsf{H}\mathbf{u}_\mathbf{a}|^2)$$
$$= \sqrt{\gamma\sigma_\mathrm{C}^2}\frac{\|\dot{\mathbf{a}}\|^2|w_1|^3}{\tilde{g}_\mathrm{T}}|\mathbf{h}^\mathsf{H}\mathbf{u}_{\dot{\mathbf{a}}}| - \sqrt{\gamma\sigma_\mathrm{C}^2}\frac{N_\mathrm{T}|w_2|^3}{\tilde{g}_\mathrm{R}}|\mathbf{h}^\mathsf{H}\mathbf{u}_\mathbf{a}|$$
$$+ \left(\frac{N_\mathrm{T}|w_2|^2}{\tilde{g}_\mathrm{R}} - \frac{\|\dot{\mathbf{a}}\|^2|w_1|^2}{\tilde{g}_\mathrm{T}}\right)|w_1||w_2||\mathbf{h}^\mathsf{H}\mathbf{u}_{\dot{\mathbf{a}}}||\mathbf{h}^\mathsf{H}\mathbf{u}_\mathbf{a}|. \quad (76)$$

As far as (74b), it can be rewritten as:

$$|w_1|^2|\mathbf{h}^\mathsf{H}\mathbf{u}_\mathrm{t}|^2 + |w_2|^2|\mathbf{h}^\mathsf{H}\mathbf{u}_\mathrm{t}|^2 + \gamma\sigma_\mathrm{C}^2 + |w_1|^2|\mathbf{h}^\mathsf{H}\mathbf{u}_{\dot{\mathbf{a}}}|^2$$
$$+ |w_2|^2|\mathbf{h}^\mathsf{H}\mathbf{u}_\mathbf{a}|^2 + 2|w_1||w_2||\mathbf{h}^\mathsf{H}\mathbf{u}_{\dot{\mathbf{a}}}||\mathbf{h}^\mathsf{H}\mathbf{u}_\mathbf{a}|$$
$$= 2\sqrt{\gamma\sigma_\mathrm{C}^2}|w_1||\mathbf{h}^\mathsf{H}\mathbf{u}_{\dot{\mathbf{a}}}| + 2\sqrt{\gamma\sigma_\mathrm{C}^2}|w_2||\mathbf{h}^\mathsf{H}\mathbf{u}_\mathbf{a}| + P_\mathrm{T}|\mathbf{h}^\mathsf{H}\mathbf{u}_\mathrm{t}|^2 \quad (77)$$

that is

$$a_1|w_1|^2 + a_2|w_2|^2 - 2b_1|w_1| - 2b_2|w_2| + 2b|w_1||w_2| = -c \quad (78)$$

where

$$a_1 \triangleq |\mathbf{h}^\mathsf{H}\mathbf{u}_\mathrm{t}|^2 + |\mathbf{h}^\mathsf{H}\mathbf{u}_{\dot{\mathbf{a}}}|^2 \quad (79a)$$
$$a_2 \triangleq |\mathbf{h}^\mathsf{H}\mathbf{u}_\mathrm{t}|^2 + |\mathbf{h}^\mathsf{H}\mathbf{u}_\mathbf{a}|^2 \quad (79b)$$
$$b_1 \triangleq \sqrt{\gamma\sigma_\mathrm{C}^2}\,|\mathbf{h}^\mathsf{H}\mathbf{u}_{\dot{\mathbf{a}}}| \quad (79c)$$
$$b_2 \triangleq \sqrt{\gamma\sigma_\mathrm{C}^2}\,|\mathbf{h}^\mathsf{H}\mathbf{u}_\mathbf{a}| \quad (79d)$$
$$b \triangleq |\mathbf{h}^\mathsf{H}\mathbf{u}_{\dot{\mathbf{a}}}||\mathbf{h}^\mathsf{H}\mathbf{u}_\mathbf{a}| \quad (79e)$$
$$c \triangleq \gamma\sigma_\mathrm{C}^2 - P_\mathrm{T}|\mathbf{h}^\mathsf{H}\mathbf{u}_\mathrm{t}|^2. \quad (79f)$$

Thus, by solving the second order (78) with respect to $|w_2|$, we have:[8]

$$|w_2| = \frac{(b_2 - b|w_1|)}{a_2} \pm \frac{\sqrt{(b_2 - b|w_1|)^2 - a_2(a_1|w_1|^2 - 2b_1|w_1| + c)}}{a_2}. \quad (80)$$

Note that:

$$a_2^2|w_2|^2 = 2(b_2 - b|w_1|)^2 - a_2(a_1|w_1|^2 - 2b_1|w_1| + c) \pm 2(b_2 - b|w_1|) \cdot \sqrt{(b_2 - b|w_1|)^2 - a_2(a_1|w_1|^2 - 2b_1|w_1| + c)} \quad (81a)$$

$$a_2^3|w_2|^3 = (b_2 - b|w_1|)^3 \pm 3(b_2 - b|w_1|)^2 \cdot \sqrt{(b_2 - b|w_1|)^2 - a_2(a_1|w_1|^2 - 2b_1|w_1| + c)} + 3(b_2 - b|w_1|) \cdot \left[(b_2 - b|w_1|)^2 - a_2(a_1|w_1|^2 - 2b_1|w_1| + c)\right] \pm \left[(b_2 - b|w_1|)^2 - a_2(a_1|w_1|^2 - 2b_1|w_1| + c)\right]^{\frac{3}{2}}$$
$$= 4(b_2 - b|w_1|)^3 - 3(b_2 - b|w_1|)a_2(a_1|w_1|^2 - 2b_1|w_1| + c) \pm [4(b_2 - b|w_1|)^2 - a_2(a_1|w_1|^2 - 2b_1|w_1| + c)] \cdot \sqrt{(b_2 - b|w_1|)^2 - a_2(a_1|w_1|^2 - 2b_1|w_1| + c)} \quad (81b)$$

$$a_2^4|w_2|^4 = \left[2(b_2 - b|w_1|)^2 - a_2(a_1|w_1|^2 - 2b_1|w_1| + c)\right]^2 - 4a_2(b_2 - b|w_1|)^2(a_1|w_1|^2 - 2b_1|w_1| + c) + 4(b_2 - b|w_1|)^4 \pm 4(b_2 - b|w_1|) \cdot \left[2(b_2 - b|w_1|)^2 - a_2(a_1|w_1|^2 - 2b_1|w_1| + c)\right] \cdot \sqrt{(b_2 - b|w_1|)^2 - a_2(a_1|w_1|^2 - 2b_1|w_1| + c)}. \quad (81c)$$

Exploiting (79) in (76) we obtain:

$$\frac{\|\dot{\mathbf{a}}\|^2|w_1|^4}{\tilde{g}_\mathrm{T}}a_1 - \frac{N_\mathrm{T}|w_2|^4}{\tilde{g}_\mathrm{R}}a_2 = \frac{\|\dot{\mathbf{a}}\|^2|w_1|^3}{\tilde{g}_\mathrm{T}}b_1 - \frac{N_\mathrm{T}|w_2|^3}{\tilde{g}_\mathrm{R}}b_2 + \left(\frac{N_\mathrm{T}|w_2|^2}{\tilde{g}_\mathrm{R}} - \frac{\|\dot{\mathbf{a}}\|^2|w_1|^2}{\tilde{g}_\mathrm{T}}\right)|w_1||w_2|b \quad (82)$$

that is

$$\frac{\tilde{g}_\mathrm{R}\|\dot{\mathbf{a}}\|^2|w_1|^4}{\tilde{g}_\mathrm{T}N_\mathrm{T}}a_1 + |w_2|^3\,b_2 = \frac{\tilde{g}_\mathrm{R}\|\dot{\mathbf{a}}\|^2|w_1|^3}{\tilde{g}_\mathrm{T}N_\mathrm{T}}b_1 + |w_2|^4\,a_2 + \left(|w_2|^2 - \frac{\tilde{g}_\mathrm{R}\|\dot{\mathbf{a}}\|^2|w_1|^2}{\tilde{g}_\mathrm{T}N_\mathrm{T}}\right)|w_1||w_2|b. \quad (83)$$

Finally, by using (80) and (81) in (82) we get the implicit (84), shown at the bottom of the next page, that can be solved numerically for $|w_1|$, which leads to $|w_2|$ via (80), and $|w_3|$ via (67c).[9] Then, the optimal beamforming weights can be computed according to (70) and (56).

2) CRB Expression With Optimal JSC Weights: Here, we use the three components of the optimal weight vector $\mathbf{w}_\mathrm{opt}$ obtained in the previous subsection to get the expression of the JSC trade-off. To this aim, we have to express both the CRB and the communication SNR as functions of w_1, w_2, and w_3. For each instantiation of the communication channel $\mathbf{h}$, the JSC tradeoff can be expressed, thanks to (49), by the following equations

$$\mathrm{CRB}(x,y) = \frac{\sigma_\mathrm{R}^2}{2L|\alpha|^2}\left(\frac{g_{\mathrm{TT}}(\theta_\mathrm{T},\theta_\mathrm{R})}{N_\mathrm{R}\|\dot{\mathbf{a}}(\theta_\mathrm{T})\|^2|w_1|^2}\right.$$

[8]The choice between the solutions with the sign plus and minus in (80) are done a-posteriori according to the non-negativity constraint of both $|w_1|$ and $|w_2|$. If both the solutions are acceptable, we choose the one which minimize the CRB.

[9]Only solutions leading to non-negative $|w_1|$, $|w_2|$, and $|w_3|$ are acceptable.

$$+\frac{g_{\mathrm{RR}}(\theta_{\mathrm{T}},\theta_{\mathrm{R}})}{N_{\mathrm{T}}\|\dot{\mathbf{b}}(\theta_{\mathrm{R}})\|^2|w_2|^2}\Bigg) \tag{85a}$$

$$\gamma=\frac{|w_1\mathbf{h}^{\mathsf{H}}\mathbf{u}_{\mathbf{a}}+w_2\mathbf{h}^{\mathsf{H}}\mathbf{u}_{\dot{\mathbf{a}}}+w_3\mathbf{h}^{\mathsf{H}}\mathbf{u}_{\mathrm{t}}|^2}{\sigma_{\mathrm{C}}^2} \tag{85b}$$

where all the other quantities can be expressed as functions of the Cartesian coordinates (instead of the angles) through the transformation Ω. Note that the phases of the weights are irrelevant for the JSC trade-off problem. Note also that the orthonormalization leads to:

$$\mathbf{u}_{\mathrm{t}}=u_0\mathbf{h}-u_1^*\mathbf{u}_{\mathbf{a}}-u_2^*\mathbf{u}_{\dot{\mathbf{a}}} \tag{86}$$

where

$$u_0\triangleq\frac{1}{\|\mathbf{h}-(\mathbf{h}^{\mathsf{H}}\mathbf{u}_{\mathbf{a}})\mathbf{u}_{\mathbf{a}}-(\mathbf{h}^{\mathsf{H}}\mathbf{u}_{\dot{\mathbf{a}}})\mathbf{u}_{\dot{\mathbf{a}}}\|} \tag{87a}$$

$$u_1\triangleq\frac{\mathbf{h}^{\mathsf{H}}\mathbf{u}_{\mathbf{a}}}{\|\mathbf{h}-(\mathbf{h}^{\mathsf{H}}\mathbf{u}_{\mathbf{a}})\mathbf{u}_{\mathbf{a}}-(\mathbf{h}^{\mathsf{H}}\mathbf{u}_{\dot{\mathbf{a}}})\mathbf{u}_{\dot{\mathbf{a}}}\|} \tag{87b}$$

$$u_2\triangleq\frac{\mathbf{h}^{\mathsf{H}}\mathbf{u}_{\dot{\mathbf{a}}}}{\|\mathbf{h}-(\mathbf{h}^{\mathsf{H}}\mathbf{u}_{\mathbf{a}})\mathbf{u}_{\mathbf{a}}-(\mathbf{h}^{\mathsf{H}}\mathbf{u}_{\dot{\mathbf{a}}})\mathbf{u}_{\dot{\mathbf{a}}}\|}. \tag{87c}$$

Thus, the SNR constraint can be re-written as

$$\gamma=\frac{w_3u_0\|\mathbf{h}\|^2+(w_1-w_3u_1)\mathbf{h}^{\mathsf{H}}\mathbf{u}_{\dot{\mathbf{a}}}+(w_2-w_3u_2)\mathbf{h}^{\mathsf{H}}\mathbf{u}_{\mathbf{a}}}{\sigma_{\mathrm{C}}^2}. \tag{88}$$

Thanks to (86) and (88), we are now able to express the JSC trade-off by means of known quantities.

D. Suboptimal Methods

The framework developed so far enables the derivation of optimal beamforming weights, taking into account power constraints and communication SNR. To circumvent the need to solve an implicit equation, we propose two suboptimal solutions that are highly effective and computationally efficient.

1) Suboptimal Method 1: Let us indicate as $\mathbf{w}_{\mathrm{opt}}^{(2)}$ the weight vector maximizing $|\mathbf{a}^{\mathsf{H}}\mathbf{w}|$ under the SNR and the power constraint. In [53] it is shown that, given the SNR constraint $\gamma=\Gamma$, it results

$$\mathbf{w}_{\mathrm{opt}}^{(2)}=\begin{cases}\sqrt{P_{\mathrm{T}}}\,\frac{\mathbf{a}}{\|\mathbf{a}\|}, & \text{if } P_{\mathrm{T}}>\frac{\Gamma N_{\mathrm{T}}\,\sigma_{\mathrm{C}}^2}{|\mathbf{h}^T\mathbf{a}|^2}\\ x_1\mathbf{u}+x_2\mathbf{a}_{\mathrm{u}}, & \text{if } \frac{\sigma_{\mathrm{C}}^2\Gamma}{\|\mathbf{h}\|^2}\le P_{\mathrm{T}}\le\frac{\Gamma N_{\mathrm{T}}\,\sigma_{\mathrm{C}}^2}{|\mathbf{h}^T\mathbf{a}|^2}\\ \sqrt{P_{\mathrm{T}}}\,\mathbf{u}, & \text{if } P_{\mathrm{T}}<\frac{\sigma_{\mathrm{C}}^2\Gamma}{\|\mathbf{h}\|^2}\end{cases} \tag{89}$$

where $\mathbf{u}\triangleq\frac{\mathbf{h}}{\|\mathbf{h}\|}$, $\mathbf{a}_{\mathrm{u}}\triangleq\frac{\mathbf{a}-(\mathbf{u}^{\mathsf{H}}\mathbf{a})\mathbf{u}}{\|\mathbf{a}-(\mathbf{u}^{\mathsf{H}}\mathbf{a})\mathbf{u}\|}$ and

$$x_1=\sqrt{\frac{\sigma_{\mathrm{C}}^2\Gamma}{\|\mathbf{h}\|^2}}\,\frac{\mathbf{u}^{\mathsf{H}}\mathbf{a}}{|\mathbf{u}^{\mathsf{H}}\mathbf{a}|},\quad x_2=\sqrt{P_{\mathrm{T}}-\frac{\sigma_{\mathrm{C}}^2\Gamma}{\|\mathbf{h}\|^2}}\,\frac{\mathbf{a}_{\mathrm{u}}{}^{\mathsf{H}}\mathbf{a}}{|\mathbf{a}_{\mathrm{u}}{}^{\mathsf{H}}\mathbf{a}|}. \tag{90}$$

If we now replace $\mathbf{a}$ by $\dot{\mathbf{a}}$, we can prove, in a way that is formally identical to that adopted in the previous subsection, that the weight vector $\mathbf{w}_{\mathrm{opt}}^{(1)}$ maximizing $|\dot{\mathbf{a}}^{\mathsf{H}}\mathbf{w}|$ under the SNR and the power constraint results in

$$\mathbf{w}_{\mathrm{opt}}^{(1)}=\begin{cases}\sqrt{P_{\mathrm{T}}}\,\frac{\dot{\mathbf{a}}}{\|\dot{\mathbf{a}}\|}, & \text{if } P_{\mathrm{T}}>\frac{\Gamma N_{\mathrm{T}}\,\sigma_{\mathrm{C}}^2}{|\mathbf{h}^T\dot{\mathbf{a}}|^2}\\ y_1\mathbf{u}+y_2\dot{\mathbf{a}}_{\mathrm{u}}, & \text{if } \frac{\sigma_{\mathrm{C}}^2\Gamma}{\|\mathbf{h}\|^2}\le P_{\mathrm{T}}\le\frac{\Gamma N_{\mathrm{T}}\,\sigma_{\mathrm{C}}^2}{|\mathbf{h}^T\dot{\mathbf{a}}|^2}\\ \sqrt{P_{\mathrm{T}}}\,\mathbf{u}, & \text{if } P_{\mathrm{T}}<\frac{\sigma_{\mathrm{C}}^2\Gamma}{\|\mathbf{h}\|^2}\end{cases} \tag{91}$$

where $\dot{\mathbf{a}}_{\mathrm{u}}\triangleq\frac{\dot{\mathbf{a}}-(\mathbf{u}^{\mathsf{H}}\dot{\mathbf{a}})\mathbf{u}}{\|\dot{\mathbf{a}}-(\mathbf{u}^{\mathsf{H}}\dot{\mathbf{a}})\mathbf{u}\|}$ and

$$y_1=\sqrt{\frac{\sigma_{\mathrm{C}}^2\Gamma}{\|\mathbf{h}\|^2}}\,\frac{\mathbf{u}^{\mathsf{H}}\dot{\mathbf{a}}}{|\mathbf{u}^{\mathsf{H}}\dot{\mathbf{a}}|},\quad y_2=\sqrt{P_{\mathrm{T}}-\frac{\sigma_{\mathrm{C}}^2\Gamma}{\|\mathbf{h}\|^2}}\,\frac{\mathbf{u}_{\dot{\mathbf{a}}}^{\mathsf{H}}\dot{\mathbf{a}}}{|\mathbf{u}_{\dot{\mathbf{a}}}^{\mathsf{H}}\dot{\mathbf{a}}|}. \tag{92}$$

Based on the CRB expression (48), we can consider the following cases, where the first two are "asymptotically optimal" solutions:

- When $\tilde{g}_{\mathrm{T}}\ll\tilde{g}_{\mathrm{R}}$, the CRB is dominated by the term $\frac{\tilde{g}_{\mathrm{R}}}{|\mathbf{a}^{\mathsf{H}}\mathbf{w}|^2}$ and thus $\mathbf{w}_{\mathrm{opt}}\to\mathbf{w}_{\mathrm{opt}}^{(2)}$.
- When $\tilde{g}_{\mathrm{T}}\gg\tilde{g}_{\mathrm{R}}$, the CRB is dominated by the term $\frac{\tilde{g}_{\mathrm{T}}}{|\dot{\mathbf{a}}^{\mathsf{H}}\mathbf{w}|^2}$ and thus $\mathbf{w}_{\mathrm{opt}}\to\mathbf{w}_{\mathrm{opt}}^{(1)}$.
- When $\tilde{g}_{\mathrm{T}}\approx\tilde{g}_{\mathrm{R}}$ the two addendum in (48) have the same relevance and we can consider $\mathbf{w}_{\mathrm{opt}}\approx\mathbf{w}_{\mathrm{opt}}^{(1)}+\mathbf{w}_{\mathrm{opt}}^{(2)}$.

2) Suboptimal Method 2: Now we present a sub-optimal method that is suitable for the whole range of possible target positions. Let us denote as $\mathbf{w}_{\mathrm{opt}}^{(\mathrm{s})}$ the weight vector which minimizes the CRB under the power constraint and regardless of the communication SNR. In Appendix A we have proven that such vector can be expressed as

$$\mathbf{w}_{\mathrm{opt}}^{(\mathrm{s})}=\sqrt{\frac{\tilde{g}_{\mathrm{T}}\,P_{\mathrm{T}}}{\tilde{g}_{\mathrm{T}}+\tilde{g}_{\mathrm{R}}}}\mathbf{u}_{\dot{\mathbf{a}}}+\sqrt{\frac{\tilde{g}_{\mathrm{R}}\,P_{\mathrm{T}}}{\tilde{g}_{\mathrm{T}}+\tilde{g}_{\mathrm{R}}}}\mathbf{u}_{\mathbf{a}}. \tag{93}$$

Let us denote with $\mathbf{w}_{\mathrm{opt}}^{(\mathrm{c})}$ the weight vector which maximizes the communication SNR under the power constraint regardless of the CRB, i.e., no guarantee for sensing performance. It is

$$\begin{aligned}
&\frac{\tilde{g}_{\mathrm{R}}\|\dot{\mathbf{a}}\|^2|w_1|^3a_2^3}{\tilde{g}_{\mathrm{T}}N_{\mathrm{T}}}(|w_1|a_1-b_1)+b_2\left[4(b_2-b|w_1|)^3-3(b_2-b|w_1|)a_2(a_1|w_1|^2-2b_1|w_1|+c)\right]\\
&\pm b_2\left[4(b_2-b|w_1|)^2-a_2(a_1|w_1|^2-2b_1|w_1|+c)\right]\sqrt{(b_2-b|w_1|)^2-a_2(a_1|w_1|^2-2b_1|w_1|+c)}\\
=\;&\left[2(b_2-b|w_1|)^2-a_2(a_1|w_1|^2-2b_1|w_1|+c)\right]^2-4a_2(b_2-b|w_1|)^2(a_1|w_1|^2-2b_1|w_1|+c)+4(b_2-b|w_1|)^4\\
&\pm 4(b_2-b|w_1|)\left[2(b_2-b|w_1|)^2-a_2(a_1|w_1|^2-2b_1|w_1|+c)\right]\sqrt{(b_2-b|w_1|)^2-a_2(a_1|w_1|^2-2b_1|w_1|+c)}\\
&+\left[2(b_2-b|w_1|)^2-a_2(a_1|w_1|^2-2b_1|w_1|+c)\pm 2(b_2-b|w_1|)\sqrt{(b_2-b|w_1|)^2-a_2(a_1|w_1|^2-2b_1|w_1|+c)}\right.\\
&\left.-\frac{\tilde{g}_{\mathrm{R}}\|\dot{\mathbf{a}}\|^2|w_1|^2a_2^2}{\tilde{g}_{\mathrm{T}}N_{\mathrm{T}}}\right]b|w_1|\left[(b_2-b|w_1|)\pm\sqrt{(b_2-b|w_1|)^2-a_2(a_1|w_1|^2-2b_1|w_1|+c)}\right]
\end{aligned} \tag{84}$$

TABLE I
BISTATIC JSC SYSTEM PARAMETERS

$N_{\mathrm{T}} = 16\,,\ \{12,\ 20,\ 24\}$	Number of Tx antennas
$N_{\mathrm{R}} = 20\,,\ \{15,\ 25,\ 30\}$	Number of Rx antennas
$P_{\mathrm{T}} = 1\,\mathrm{W}$	Tx power
$\lvert\alpha\rvert = 0.0015$	Reflection coefficient
$L = 30$	Number of Tx symbols
$\theta_{\mathrm{T}} = \{\pi/3,\ \pi/6\}$	Angle of departure
$\theta_{\mathrm{R}} = \{\pi/3,\ \pi/6\}$	Angle of arrival
h_i with $i = 1, 2, \ldots N_{\mathrm{T}}$	Tx-UE channel coefficients
$h_i \sim \mathcal{CN}(0, 1)$	for Rayleigh fading
$h_i \sim \mathcal{CN}(1, 1)$	for Rice fading
$\sigma_{\mathrm{C}}^2 = 0\,\mathrm{dBm}$	Noise power at the UE Rx (comm.)
$\sigma_{\mathrm{R}}^2 = 0\,\mathrm{dBm}$	Noise power at the bistatic Rx (sensing)

immediate that

$$\mathbf{w}_{\mathrm{opt}}^{(\mathrm{c})} = \sqrt{P_{\mathrm{T}}}\frac{\mathbf{h}}{\|\mathbf{h}\|}. \tag{94}$$

Now, by defining the suboptimal beamforming vector

$$\mathbf{w}_{\mathrm{bal}} \triangleq (1-\nu)\ \mathbf{w}_{\mathrm{opt}}^{(\mathrm{s})} + \nu\ \mathbf{w}_{\mathrm{opt}}^{(\mathrm{c})} \tag{95}$$

we can set a trade-off between sensing and communication by varying the parameter $\nu \in [0, 1]$.

Remark: In terms of complexity comparison, we note that the optimal solution involves solving the implicit (84),[10] while the suboptimal ones only require the direct computation of two vectors (i.e., (91) and (89) for the Suboptimal Method 1, (94) and (93) for the Suboptimal Method 2) which have the same complexity as the optimal solution for the monostatic case [53].

V. NUMERICAL RESULTS

This section presents the numerical results derived from the developed analytical framework.

The parameters defining such a scenario are summarized in Table I.[11] To generalize the results, both the spatial coordinates and the root CRB are normalized relative to the baseline l, which does not require explicit specification here. The target localization error is computed based on the normalized version of (47) relative to the squared baseline l^2. This is followed by a square root operation, hereafter referred to as the normalized root CRB. This bound is subsequently averaged over 10^4 realizations of the channel vector $\mathbf{h}$, characterized by i.i.d. complex Gaussian random entries with unit variance, and mean zero (Rayleigh fading) or one (Rice fading with Rice factor 1). It should be specified that the optimization algorithms (both optimal and suboptimal) are computed based on each specific channel realization, and only afterward are the resulting CRB values averaged over the various realizations.

A. JSC Optimal Trade-Off

In this subsection, we analyze the JSC trade-off in terms of localization CRB versus communication SNR, with a target at 3 different positions such that: a) $\theta_{\mathrm{R}} = \pi/3$, $\theta_{\mathrm{T}} = \pi/6$ b) $\theta_{\mathrm{R}} = \theta_{\mathrm{T}} = \pi/3$, and c) $\theta_{\mathrm{R}} = \pi/6$, $\theta_{\mathrm{T}} = \pi/3$.

[10] (84) is efficiently solvable numerically using standard root-finding methods and poses no practical computational burden on modern processors.

[11] Instead of calculating α as a function of distance, according to (6), we preferred to use a value consistent with [9] for comparison purposes.

1) JSC Optimal Trade-Off in NLoS Single User Scenario: In Fig. 3, we illustrate the normalized root CRB as a function of the required communication SNR γ, considering $\mathbf{w} = \mathbf{w}_{\mathrm{opt}}$ in a NLoS scenario (Rayleigh communication channel model). Here, $\mathbf{w}_{\mathrm{opt}}$ denotes the optimal solution, analytically derived using equations (56), (67c), (80), and (82). For a comprehensive comparative analysis, we also present results for the case $\mathbf{w} = \mathbf{w}_{\mathrm{sub}}$, defined by

$$\mathbf{w}_{\mathrm{sub}} = \frac{c_1}{c_0}\mathbf{w}_{\mathrm{opt}}^{(1)} + \frac{c_2}{c_0}\mathbf{w}_{\mathrm{opt}}^{(2)} \tag{96}$$

where $\mathbf{w}_{\mathrm{sub}}$ is the weight vector computed using the suboptimal method 1, as detailed in Sec. IV-D1, i.e., $\mathbf{w}_{\mathrm{opt}}^{(1)}$ and $\mathbf{w}_{\mathrm{opt}}^{(2)}$ are defined by (91) and (89), respectively. Note that c_0 is a normalization constant such that $\|\mathbf{w}_{\mathrm{sub}}\|^2 = P_{\mathrm{T}}$ and different values of c_1 and c_2 are under consideration. First, it has to be noticed that, according to (5), the actual communication SNR attained by the choice $\mathbf{w} = \mathbf{w}_{\mathrm{sub}}$ result in $\|\mathbf{h}^H\mathbf{w}_{\mathrm{sub}}\|^2/\sigma_{\mathrm{C}}^2$ that, in general, is different than Γ. It is evident that, through a discerning selection of c_1 and c_2 (as discussed in Sec. IV-D1), the suboptimal method 1 closely approximates the performance of the optimal method in the various scenarios of target position. More specifically, in the scenario of Fig. 3(a) ($\theta_{\mathrm{R}} = \pi/3$, $\theta_{\mathrm{T}} = \pi/6$) the target position is such that $\tilde{g}_{\mathrm{T}} > \tilde{g}_{\mathrm{R}}$ (please refer to Fig. 2). Thus it is not surprising that the suboptimal method 1 with $c_1 > c_2$ is the choice that best approximates the optimal method. In the scenario of Fig. 3(b) ($\theta_{\mathrm{R}} = \theta_{\mathrm{T}} = \pi/3$), instead, the target is in a position where (always according with Fig. 2) $\tilde{g}_{\mathrm{T}} = \tilde{g}_{\mathrm{R}}$. As a consequence, the suboptimal method 1 with $c_1 = c_2$ is the choice that best approximate the optimal method. Finally, in Fig. 3(c) ($\theta_{\mathrm{R}} = \pi/6$, $\theta_{\mathrm{T}} = \pi/3$) the target position is such that $\tilde{g}_{\mathrm{T}} < \tilde{g}_{\mathrm{R}}$. Thus the suboptimal method 1 with the choice $c_1 < c_2$ is the best approximation. In all these cases, we note that the proposed analytical optimal solution is available only in a certain range of required communication SNR Γ. Within such a range, the communication performance can improve with a negligible degradation of the CRB. If higher values of γ are required, the suboptimal method 1 can be adopted with a proper choice of $c_1,\ c_2$ as previously discussed.

When comparing the suboptimal and optimal cases in the figures, the line representing the root CRB for the optimal solution may vanish beyond a certain SNR value. This occurs because the SNR constraint becomes excessively stringent, making it infeasible to minimize the CRB further.

2) JSC Optimal Trade-Off in LoS Single User Scenario: In Fig. 4, the normalized root CRB is still depicted as a function of the required communication SNR γ, considering $\mathbf{w} = \mathbf{w}_{\mathrm{opt}}$, but a LoS scenario (Rice communication channel model, with a Rice factor equal to 1) is considered instead of a NLoS as in Fig. 3. The same considerations made previously can be applied to cases a), b), and c). Furthermore, by comparing Fig. 4 to Fig. 3 it can be observed that in all considered cases, the LoS situation implies a significantly smaller increase in localization error for the same required SNR. For example, in the NLoS case, the curves corresponding to the suboptimal method exhibit an almost exponential increase in the CRB beyond a certain value of the required SNR, whereas in the LoS case, even the suboptimal cases show a relatively flat trend similar to that of the optimal case. This is in line with intuition: in the case of less severe attenuation of the communication channel, the beamforming orientation required for localization nonetheless attenuates the communication SNR to a lesser extent.

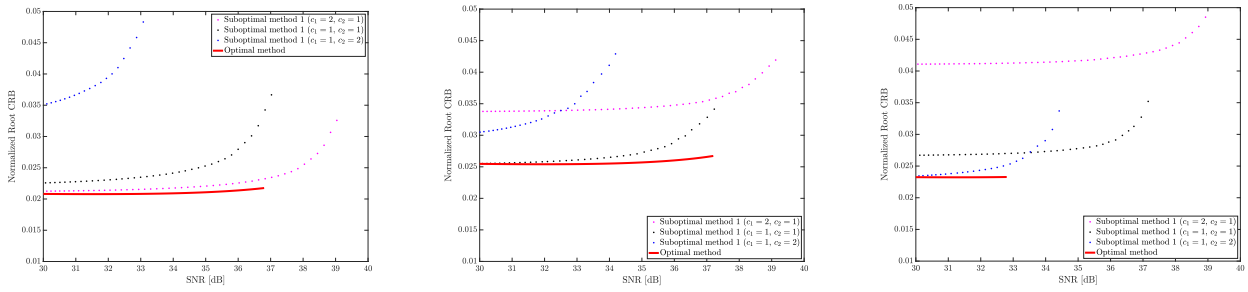

(a) (b) (c)

Fig. 3. Optimal MIMO vs suboptimal in single user case. Normalized root CRB vs communication SNR in NLoS scenario (Rayleigh channel) for: (a) $\theta_R = \pi/3$, $\theta_T = \pi/6$ (b) $\theta_R = \theta_T = \pi/3$ and (c) $\theta_R = \pi/6$, $\theta_T = \pi/3$.

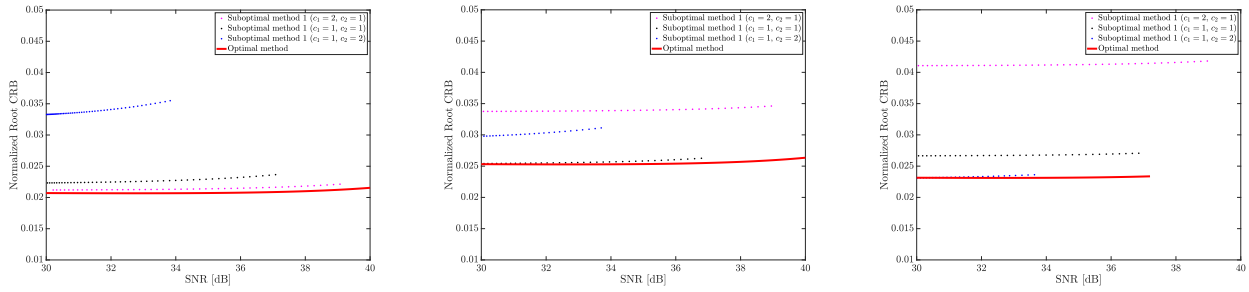

(a) (b) (c)

Fig. 4. Optimal MIMO vs suboptimal in single user case. Normalized root CRB vs communication SNR in LoS scenario (Rice channel) for: (a) $\theta_R = \pi/3$, $\theta_T = \pi/6$ (b) $\theta_R = \theta_T = \pi/3$ and (c) $\theta_R = \pi/6$, $\theta_T = \pi/3$.

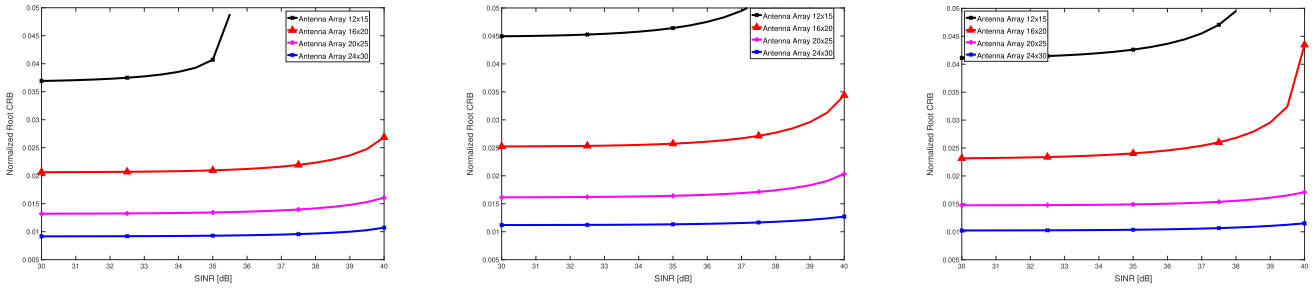

(a) (b) (c)

Fig. 5. Optimal MIMO with single user. Normalized root CRB vs communication SNR in NLoS scenario (Rayleigh channel) for: (a) $\theta_R = \pi/3$, $\theta_T = \pi/6$ (b) $\theta_R = \theta_T = \pi/3$ and (c) $\theta_R = \pi/6$, $\theta_T = \pi/3$. The effect of increasing the number of antennas.

The effect of the number of antennas: In Fig. 5, we observe the effect of increasing the number of antennas both at the transmitter and the receiver while keeping their ratio fixed (in this case, 4 : 5). The cases considered correspond to a number of transmitting and receiving antennas of (12,15), (16,20), (20,25), and (24,30), respectively. As expected, for a fixed communication SNR requirement, the CRB on the localization error decreases as the number of antennas increases. This confirms that system performance scales with the number of antennas. Increasing N_T and/or N_R leads to larger matrix sizes, which can increase computation time—especially in the multiuser case involving SDP. However, due to the convexity of the problem, efficient solvers remain practical even for larger dimensions. In the single-user case, the complexity increase is minimal, as the main step reduces to solving a scalar equation.

3) JSC Optimal Trade-Off in LoS Multi User Scenario: In this subsection, we present the results for the multi-user case. Fig. 6 shows the trade-off between the normalized root CRB and the minimum SINR required for each user (assumed to be the same for all K users). For a fair comparison, we consider a Rayleigh channel as in the single-user NLoS scenario of Fig. 3. Cases a), b), and c) refer to the same target positions defined in the corresponding cases considered for the single-user scenario. By comparing Fig. 3(a) to 6(a), 3(b) to 6(b), and 3(c) to 6(c), we can observe that, for $K = 1$, the SDP method obviously provides the same results as the analytical optimization. Indeed, the normalized root CRB values are slightly above 0.02in case a), around 0.025in case b), and between 0.02 and 0.025 in case c), remaining nearly constant up to SNR values of about 32–33 dB (as was also the case with the analytical optimization in Fig. 3). Note that for $K = 1$ the SINR clearly reduces to the SNR. For $K = 2$, 4, and 8, we observe that, for the same communication SINR required for each user, the minimum achievable normalized root CRB increases progressively due to the growing number of

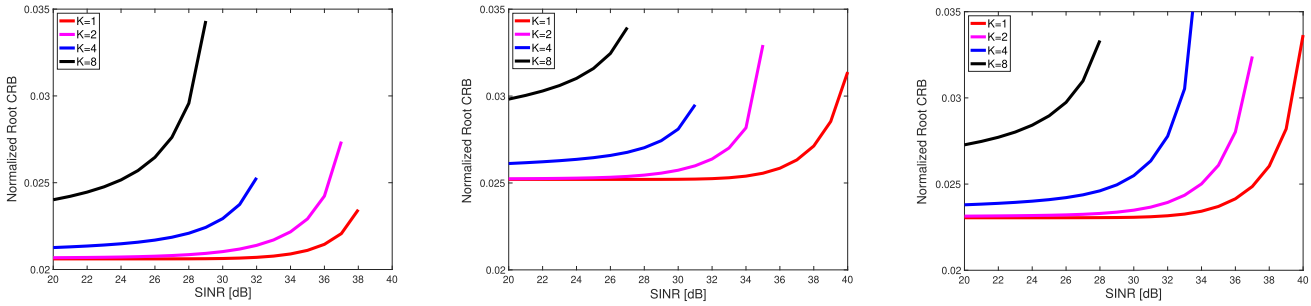

Fig. 6. Optimal MIMO with K users. Normalized root CRB vs communication SNR in NLoS scenario (Rayleigh channel) for: (a) $\theta_R = \pi/3$, $\theta_T = \pi/6$ (b) $\theta_R = \theta_T = \pi/3$ and (c) $\theta_R = \pi/6$, $\theta_T = \pi/3$.

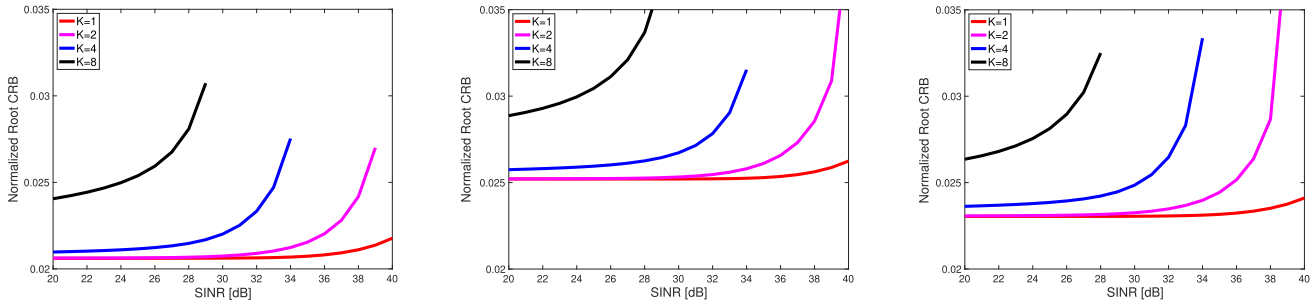

Fig. 7. Optimal MIMO with K users. Normalized root CRB vs communication SNR in LoS scenario (Rice channel) for: (a) $\theta_R = \pi/3$, $\theta_T = \pi/6$ (b) $\theta_R = \theta_T = \pi/3$ and (c) $\theta_R = \pi/6$, $\theta_T = \pi/3$.

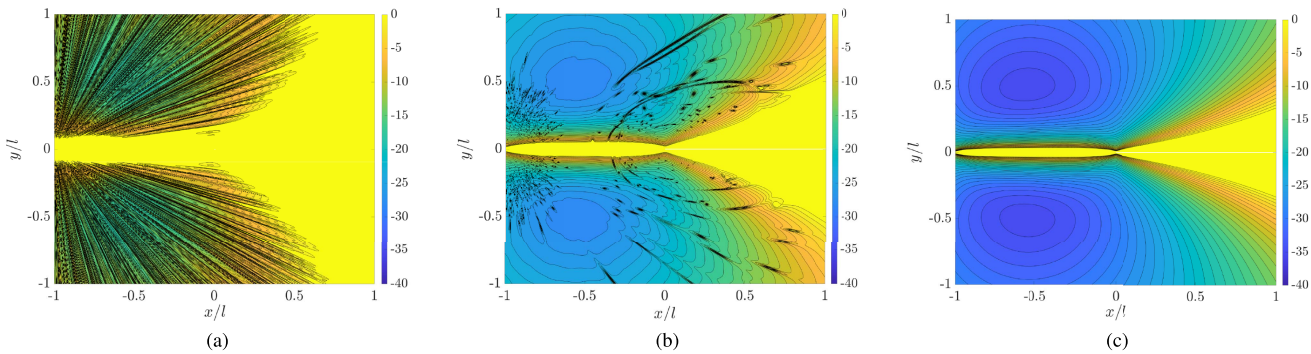

Fig. 8. Normalized CRB in dB as a function of the target normalized position for: (a) communication optimal weight vector (94); (b) JSC "balanced" weight vector (95) with $\nu = 0.5$ and (c) sensing optimal weight vector (93). NLoS scenario (Rayleigh channel).

constraints imposed on the optimization. For example, requiring an SINR of 30 dB with two users does not significantly increase the minimum achievable normalized root CRB (compared to the case where an SINR of 30 dB required for a single user); however, with $K = 4$ the increase becomes clearly noticeable, and with $K = 8$ the problem becomes infeasible (for such SINR levels required for all users).

4) JSC Optimal Trade-Off in NLoS Multi User Scenario: In Fig. 7, the normalized root CRB is still depicted as a function of the required communication SINR for each user, but a LoS scenario (Rice communication channel model, with a Rice factor equal to 1) is considered instead of a NLoS as in Fig. 3. If we compare Fig. 7 with Fig. 4 (related to the NLoS case with a single user), we can still recognize the validity of the considerations made in the previous subsection regarding the impact of requiring a minimum SINR for an increasing number of users on the minimum achievable normalized root CRB. These considerations hold for all the target positions a), b), and c). Furthermore, by comparing Fig. 7 to Fig. 6 it can be observed that in all considered cases, the LoS situation implies a significantly smaller increase in localization error for the same required SINR (exactly as could be observed by comparing the NLoS scenario with the LoS scenario in the single-user case). These results are consistent with what was reasonably expected and strengthen the idea of the robustness of the optimization models used in both the single-user and multi-user cases.

B. CRB as a Function of the Target Position

We now analyze the JSC trade-off of the MIMO bistatic configuration for different target locations when the beamforming vector is optimized:

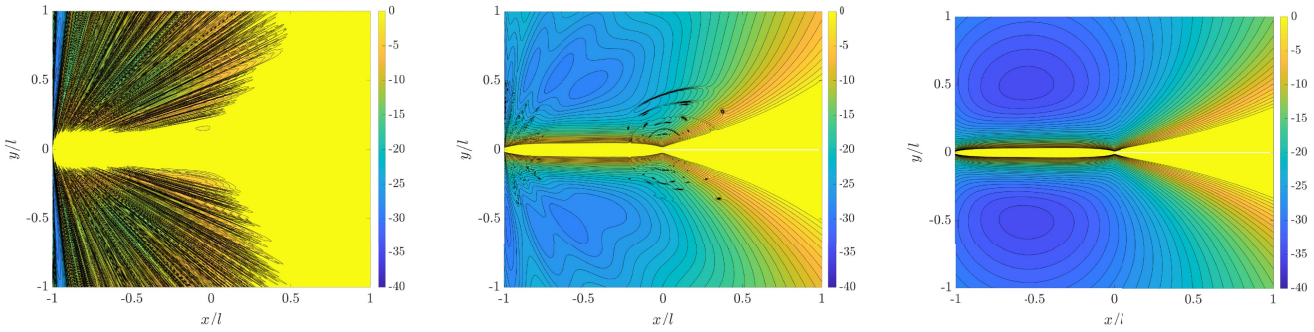

Fig. 9. Normalized CRB in dB as a function of the target normalized position for: (a) communication optimal weight vector (94); (b) JSC "balanced" weight vector (95) with $\nu = 0.5$ and (c) sensing optimal weight vector (93). LoS scenario (Rice channel).

i) for communication purposes only;
ii) for sensing purposes only;
iii) by balancing communication and sensing according to suboptimal method 2.

In Fig. 8(a), the normalized root CRB as a function of the target position (x, y) is plotted with a weight vector choice that is optimal for communication purposes ($\mathbf{w} = \sqrt{P_{\mathrm{T}}}\frac{\mathbf{h}}{\|\mathbf{h}\|}$), referred to as case a). We can note that the target positions for which the CRB on localization error is acceptable (below 10^{-2}, i.e, -20 dB) do not include large portions of the area, e.g., all positions with $x \in [-0.2\,\mathrm{l},\ 0.2\,\mathrm{l}]$ or $y < 0.6\,\mathrm{l}$. In Fig. 8(b), the normalized CRB as a function of the target position (x, y) is plotted, instead, with a JSC "balanced" weight vector choice based on the suboptimal method 2 described in Sec. IV-D2 ($\mathbf{w}$ as in (95) with $\nu = 0.5$ that takes both sensing and communication functionalities into account. This is referred to as case b). As expected, the portion of the space for which the target localization normalized CRB is under 10^{-2} (i.e., -20dB) has an intermediate area between the cases of Figs. 8(a) (optimal for communication) and 8(c) (optimal for sensing). Finally, in Fig. 8(c), the normalized CRB as a function of the target position (x, y) is plotted, with a weight vector choice that is optimal for sensing ($\mathbf{w} = \sqrt{\frac{P_{\mathrm{T}}\,\tilde{g}_{\mathrm{T}}}{\tilde{g}_{\mathrm{T}}+\tilde{g}_{\mathrm{R}}}}\mathbf{u}_{\dot{\mathbf{a}}} + \sqrt{\frac{P_{\mathrm{T}}\,\tilde{g}_{\mathrm{R}}}{\tilde{g}_{\mathrm{T}}+\tilde{g}_{\mathrm{R}}}}\mathbf{u}_{\mathbf{a}}$), referred to as case c). In this case, the region where the CRB on localization error is acceptable covers almost the entire area, except for a zone near the baseline and an approximately triangular section with vertices at (0,0), $(-0.2l, -l)$, and $(0.2l, -l)$. In Figs. 9(a), 9(b), and 9(c) the same three situations as in the previous cases a), b), and c) are represented, with the only difference being that now the communication channel vector $\mathbf{h}$ follows a Rice model instead of a Rayleigh one, with Rice factor equal to 1. The same considerations as before apply, with the additional note that, with respect Fig. 3, the normalized CRB values are pointwise different in cases a) and b) (where the weight vector also depends on the coefficient $\mathbf{h}$ of the communication channel) and identical in case c) (where the weight vector does not depend on $\mathbf{h}$).

VI. Conclusion

In this work, we investigated the fundamental limits of a bistatic JSC MIMO system in terms of the CRB for position estimation and its dependency on the beamforming vector at the transmitter. The problem of minimizing the CRB under power and communication SNR constraints was analytically solved in the case of single user, and an exact solution for the optimal weight vector was derived. Additionally, two suboptimal methods were proposed, demonstrating performance close to the optimal solution across a wide range of practical scenarios. The exact and suboptimal methods were validated through simulations, highlighting their effectiveness in addressing the trade-off between sensing and communication functionalities in bistatic systems. Moreover, in the numerical results, different numbers of transmit and receive antennas have been included to illustrate the performance scalability of the proposed solution when increasing array sizes. Finally, a SDP-based solution is provided for the optimal beamforming vector, which minimizes the CRB under power and communication SINR constraints in the presence of multiple users. These findings enable a precise characterization of the trade-off between communication and sensing in multi-antenna bistatic configurations, represented as the minimum achievable CRB on target localization error for a given communication SNR (in the single user case) and SINR (in the multiuser case), or vice versa. This trade-off is further influenced by key system parameters, including target position, antenna geometry, power constraints, and channel characteristics. Moreover, the proposed approach can be leveraged to generate localization error maps, providing predictions of localization performance based on the target's position. This capability offers a valuable tool for network designers, enabling informed planning and optimization of bistatic JSC systems.

Appendix

If we do not have any constraint on the communication SNR, we can consider $\lambda = 0$ in (59), thus obtaining:

$$|w_1|^2 = \frac{1}{\|\dot{\mathbf{a}}\|}\sqrt{\frac{\tilde{g}_{\mathrm{T}}}{\mu}} \tag{97a}$$

$$|w_2|^2 = \sqrt{\frac{\tilde{g}_{\mathrm{R}}}{\mu N_{\mathrm{T}}}} \tag{97b}$$

$$w_3 = 0\,. \tag{97c}$$

The multiplier μ can be derived by observing that (57c) with $w_3 = 0$ leads to $|w_1|^2 + |w_2|^2 = P_{\mathrm{T}}$. By substituting such a condition in (97) we readily obtain $\sqrt{\mu} = \frac{\sqrt{\frac{\tilde{g}_{\mathrm{T}}}{\|\dot{\mathbf{a}}\|^2}}+\sqrt{\frac{\tilde{g}_{\mathrm{R}}}{N_{\mathrm{T}}}}}{P_{\mathrm{T}}}$ and thus

the solution:

$$|w_1|^2 = \frac{\tilde{g}'_{\mathrm{T}}}{\tilde{g}'_{\mathrm{T}} + \tilde{g}'_{\mathrm{R}}} P_{\mathrm{T}} \tag{98a}$$

$$|w_2|^2 = \frac{\tilde{g}'_{\mathrm{R}}}{\tilde{g}'_{\mathrm{T}} + \tilde{g}'_{\mathrm{R}}} P_{\mathrm{T}} \tag{98b}$$

$$w_3 = 0\,. \tag{98c}$$

where we defined $\tilde{g}'_{\mathrm{T}} \triangleq \sqrt{\frac{\tilde{g}_{\mathrm{T}}}{\|\dot{\mathbf{a}}\|^2}}$ and $\tilde{g}'_{\mathrm{R}} \triangleq \sqrt{\frac{\tilde{g}_{\mathrm{R}}}{N_{\mathrm{T}}}}$. We can observe that such a solution does not depend on the weights' phases. The CRB in (85) results in

$$\begin{aligned}\mathrm{CRB}(x,y) &= \frac{(\tilde{g}'_{\mathrm{T}})^2}{|w_1|^2} + \frac{(\tilde{g}'_{\mathrm{R}})^2}{|w_2|^2} = \frac{(\tilde{g}_{\mathrm{T}} + \tilde{g}_{\mathrm{R}})}{P_{\mathrm{T}}} \\ &= \frac{\sigma_{\mathrm{R}}^2}{2L|\alpha|^2 P_{\mathrm{T}}} \left(\sqrt{\frac{g_{\mathrm{TT}}(\theta_{\mathrm{T}}, \theta_{\mathrm{R}})}{N_{\mathrm{R}} \|\dot{\mathbf{a}}(\theta_{\mathrm{T}})\|^2}} + \sqrt{\frac{g_{\mathrm{RR}}(\theta_{\mathrm{T}}, \theta_{\mathrm{R}})}{N_{\mathrm{T}} \|\dot{\mathbf{b}}(\theta_{\mathrm{R}})\|^2}} \right)^2 .\end{aligned} \tag{99}$$

REFERENCES

[1] F. Zabini, E. Paolini, W. Xu, and A. Giorgetti, "Joint sensing and communication with multiple antennas and bistatic configuration," in *Proc. IEEE Int. Conf. Commun. Workshops*, 2023, pp. 1416–1421.

[2] Z. Zhuang, D. Wen, Y. Shi, G. Zhu, S. Wu, and D. Niyato, "Integrated sensing-communication-computation for over-the-air edge AI inference," *IEEE Trans. Wireless Commun.*, vol. 23, no. 4, pp. 3205–3220, Apr. 2024.

[3] K. Wu, J. A. Zhang, X. Huang, and Y. J. Guo, "OTFS-based joint communication and sensing for future industrial IoT," *IEEE Internet Things J.*, vol. 10, no. 3, pp. 1973–1989, Feb. 2023.

[4] X. Chen, Z. Feng, Z. Wei, P. Zhang, and X. Yuan, "Code-division OFDM joint communication and sensing system for 6G machine-type communication," *IEEE Internet Things J.*, vol. 8, no. 15, pp. 12093–12105, Aug. 2021.

[5] S. D. Liyanaarachchi, T. Riihonen, C. B. Barneto, and M. Valkama, "Optimized waveforms for 5G–6G communication with sensing: Theory, simulations and experiments," *IEEE Trans. Wireless Commun.*, vol. 20, no. 12, pp. 8301–8315, Dec. 2021.

[6] T. Wild, V. Braun, and H. Viswanathan, "Joint design of communication and sensing for beyond 5G and 6G systems," *IEEE Access*, vol. 9, pp. 30845–30857, 2021.

[7] Q. Qi, X. Chen, A. Khalili, C. Zhong, Z. Zhang, and D. W. K. Ng, "Integrating sensing, computing, and communication in 6G wireless networks: Design and optimization," *IEEE Trans. Commun.*, vol. 70, no. 9, pp. 6212–6227, Sep. 2022.

[8] U. Demirhan and A. Alkhateeb, "Integrated sensing and communication for 6G: Ten key machine learning roles," *IEEE Commun. Mag.*, vol. 61, no. 5, pp. 113–119, May 2023.

[9] X. Fang, W. Feng, Y. Chen, N. Ge, and Y. Zhang, "Joint communication and sensing toward 6G: Models and potential of using MIMO," *IEEE Internet Things J.*, vol. 10, no. 5, pp. 4093–4116, Mar. 2023.

[10] M. Ashraf, B. Tan, D. Moltchanov, J. S. Thompson, and M. Valkama, "Joint optimization of radar and communications performance in 6G cellular systems," *IEEE Trans. Green Commun. Netw.*, vol. 7, no. 1, pp. 522–536, Mar. 2023.

[11] M. A. Hossain, A. Xiang, A. Kiani, T. Saboorian, J. Kaippallimalil, and N. Ansari, "AI-assisted E2E network slicing for integrated sensing and communication in 6G networks," *IEEE Internet Things J.*, vol. 11, no. 6, pp. 10627–10634, Mar. 2024.

[12] M. L. Rahman, J. A. Zhang, X. Huang, Y. J. Guo, and R. W. Heath, "Framework for a perceptive mobile network using joint communication and radar sensing," *IEEE Trans. Aerosp. Electron. Syst.*, vol. 56, no. 3, pp. 1926–1941, Jun. 2020.

[13] D. Ma, N. Shlezinger, T. Huang, Y. Liu, and Y. C. Eldar, "Joint radar-communication strategies for autonomous vehicles: Combining two key automotive technologies," *IEEE Signal Process. Mag.*, vol. 37, no. 4, pp. 85–97, Jul. 2020.

[14] H. Ma, Z. Wei, Z. Li, F. Ning, X. Chen, and Z. Feng, "Performance of cooperative detection in joint communication-sensing vehicular network: A data analytic and stochastic geometry approach," *IEEE Trans. Veh. Technol.*, vol. 72, no. 3, pp. 3848–3863, Mar. 2023.

[15] L. Shi, B. Béchadergue, L. Chassagne, and H. Guan, "Joint visible light sensing and communication using m-CAP modulation," *IEEE Trans. Broadcast.*, vol. 69, no. 1, pp. 276–288, Mar. 2023.

[16] Z. Zhou, X. Li, C. You, K. Huang, and Y. Gong, "Joint sensing and communication-rate control for energy efficient mobile crowd sensing," *IEEE Trans. Wireless Commun.*, vol. 22, no. 2, pp. 1314–1327, Feb. 2023.

[17] X. Li, G. Feng, Y. Liu, S. Qin, and Z. Zhang, "Joint sensing, communication, and computation in mobile crowdsensing enabled edge networks," *IEEE Trans. Wireless Commun.*, vol. 22, no. 4, pp. 2818–2832, Apr. 2023.

[18] A. Hassanien, M. G. Amin, Y. D. Zhang, and F. Ahmad, "Signaling strategies for dual-function radar communications: An overview," *IEEE Aerosp. Electron. Syst. Mag.*, vol. 31, no. 10, pp. 36–45, Oct. 2016.

[19] L. Zheng, M. Lops, Y. C. Eldar, and X. Wang, "Radar and communication coexistence: An overview: A review of recent methods," *IEEE Signal Process. Mag.*, vol. 36, no. 5, pp. 85–99, Sep. 2019.

[20] X. Chen, Z. Feng, Z. Wei, F. Gao, and X. Yuan, "Performance of joint sensing-communication cooperative sensing UAV network," *IEEE Trans. Veh. Technol.*, vol. 69, no. 12, pp. 15545–15556, Dec. 2020.

[21] J. A. Zhang et al., "An overview of signal processing techniques for joint communication and radar sensing," *IEEE J. Sel. Topics Signal Process.*, vol. 15, no. 6, pp. 1295–1315, Nov. 2021.

[22] L. Pucci, E. Paolini, and A. Giorgetti, "System-level analysis of joint sensing and communication based on 5G new radio," *IEEE J. Sel. Areas Commun.*, vol. 40, no. 7, pp. 2043–2055, Jul. 2022.

[23] C. B. Barneto, T. Riihonen, S. D. Liyanaarachchi, M. Heino, N. González-Prelcic, and M. Valkama, "Beamformer design and optimization for joint communication and full-duplex sensing at mm-Waves," *IEEE Trans. Commun.*, vol. 70, no. 12, pp. 8298–8312, Dec. 2022.

[24] Q. Huang, Z. Luo, J. Zhang, W. Wang, and Q. Zhang, "LoRadar: Enabling concurrent radar sensing and LoRa communication," *IEEE Trans. Mobile Comput.*, vol. 21, no. 6, pp. 2045–2057, Jun. 2022.

[25] J. A. Zhang et al., "Enabling joint communication and radar sensing in mobile networks—A survey," *IEEE Commun. Surveys Tuts.*, vol. 24, no. 1, pp. 306–345, Firstquarter 2022.

[26] J. Chu, R. Liu, M. Li, Y. Liu, and Q. Liu, "Joint secure transmit beamforming designs for integrated sensing and communication systems," *IEEE Trans. Veh. Technol.*, vol. 72, no. 4, pp. 4778–4791, Apr. 2023.

[27] Z. Ni, J. A. Zhang, K. Yang, X. Huang, and T. A. Tsiftsis, "Multi-metric waveform optimization for multiple-input single-output joint communication and radar sensing," *IEEE Trans. Commun.*, vol. 70, no. 2, pp. 1276–1289, Feb. 2022.

[28] Z. Wei, H. Qu, W. Jiang, K. Han, H. Wu, and Z. Feng, "Iterative signal processing for integrated sensing and communication systems," *IEEE Trans. Green Commun. Netw.*, vol. 7, no. 1, pp. 401–412, Mar. 2023.

[29] C. Giovannetti, N. Decarli, S. Bartoletti, R. A. Stirling-Gallacher, and B. M. Masini, "Target positioning accuracy of V2X sidelink joint communication and sensing," *IEEE Wireless Commun. Lett.*, vol. 13, no. 3, pp. 849–853, Mar. 2024.

[30] S. Bartoletti et al., "Integration of sensing and localization in V2X sidelink communications," *IEEE Commun. Mag.*, vol. 62, no. 8, pp. 185–191, Aug. 2024.

[31] N. Decarli, A. Guerra, C. Giovannetti, F. Guidi, and B. M. Masini, "V2X sidelink localization of connected automated vehicles," *IEEE J. Sel. Areas Commun.*, vol. 42, no. 1, pp. 120–133, Jan. 2024.

[32] N. Decarli, S. Bartoletti, A. Bazzi, R. A. Stirling-Gallacher, and B. M. Masini, "Performance characterization of joint communication and sensing with beyond 5G NR-V2X sidelink," *IEEE Trans. Veh. Technol.*, vol. 73, no. 7, pp. 10044–10059, Jul. 2024.

[33] A. Elzanaty, J. Liu, A. Guerra, F. Guidi, Y. Ma, and R. Tafazolli, "Near and far field model mismatch: Implications on 6G communications, localization, and sensing," *IEEE Internet Things Mag.*, vol. 7, no. 5, pp. 120–126, Sep. 2024.

[34] C. Dou, N. Huang, Y. Wu, L. Qian, and T. Q. S. Quek, "Channel sharing aided integrated sensing and communication: An energy-efficient sensing scheduling approach," *IEEE Trans. Wireless Commun.*, vol. 23, no. 5, pp. 4802–4814, May 2024.

[35] R. Li, Z. Xiao, and Y. Zeng, "Toward seamless sensing coverage for cellular multi-static integrated sensing and communication," *IEEE Trans. Wireless Commun.*, vol. 23, no. 6, pp. 5363–5376, Jun. 2024.

[36] C. Diaz-Vilor, M. A. Almasi, A. M. Abdelhady, A. Celik, A. M. Eltawil, and H. Jafarkhani, "Sensing and communication in UAV cellular networks: Design and optimization," *IEEE Trans. Wireless Commun.*, vol. 23, no. 6, pp. 5456–5472, Jun. 2024.
[37] K. Wu, J. A. Zhang, Z. Ni, X. Huang, Y. J. Guo, and S. Chen, "Joint communications and sensing employing optimized MIMO-OFDM signals," *IEEE Internet Things J.*, vol. 11, no. 6, pp. 10368–10383, Mar. 2024.
[38] Z. Wei et al., "Symbol-level integrated sensing and communication enabled multiple base stations cooperative sensing," *IEEE Trans. Veh. Technol.*, vol. 73, no. 1, pp. 724–738, Jan. 2024.
[39] S. P. Chepuri, N. Shlezinger, F. Liu, G. C. Alexandropoulos, S. Buzzi, and Y. C. Eldar, "Integrated sensing and communications with reconfigurable intelligent surfaces: From signal modeling to processing," *IEEE Signal Process. Mag.*, vol. 40, no. 6, pp. 41–62, Sep. 2023.
[40] Z. Yu et al., "Active RIS-aided ISAC systems: Beamforming design and performance analysis," *IEEE Trans. Commun.*, vol. 72, no. 3, pp. 1578–1595, Mar. 2024.
[41] Z. Yu et al., "Addressing the mutual interference in uplink ISAC receivers: A projection method," *IEEE Wireless Commun. Lett.*, vol. 13, no. 11, pp. 3109–3113, Nov. 2024.
[42] X. Tong, Z. Zhang, J. Wang, C. Huang, and M. Debbah, "Joint multi-user communication and sensing exploiting both signal and environment sparsity," *IEEE J. Sel. Topics Signal Process.*, vol. 15, no. 6, pp. 1409–1422, Nov. 2021.
[43] C. Chaccour, M. N. Soorki, W. Saad, M. Bennis, P. Popovski, and M. Debbah, "Seven defining features of terahertz (THz) wireless systems: A fellowship of communication and sensing," *IEEE Commun. Surveys Tuts.*, vol. 24, no. 2, pp. 967–993, Secondquarter 2022.
[44] T. Mao, J. Chen, Q. Wang, C. Han, Z. Wang, and G. K. Karagiannidis, "Waveform design for joint sensing and communications in millimeter-wave and low terahertz bands," *IEEE Trans. Commun.*, vol. 70, no. 10, pp. 7023–7039, Oct. 2022.
[45] A. Colpaert, S. De Bast, R. Beerten, A. P. Guevara, Z. Cui, and S. Pollin, "Massive MIMO channel measurement data set for localization and communication," *IEEE Commun. Mag.*, vol. 61, no. 9, pp. 114–120, Sep. 2023.
[46] K. Wu, J. A. Zhang, X. Huang, R. W. Heath, and Y. J. Guo, "Green joint communications and sensing employing analog multi-beam antenna arrays," *IEEE Commun. Mag.*, vol. 61, no. 7, pp. 172–178, Jul. 2023.
[47] E. Fishler, A. Haimovich, R. Blum, D. Chizhik, L. Cimini, and R. Valenzuela, "MIMO radar: An idea whose time has come," in *Proc. 2004 IEEE Radar Conf.*, 2004, pp. 71–78.
[48] I. Bekkerman and J. Tabrikian, "Target detection and localization using MIMO radars and sonars," *IEEE Trans. Signal Process.*, vol. 54, no. 10, pp. 3873–3883, Oct. 2006.
[49] P. Khomchuk, R. S. Blum, and I. Bilik, "Performance analysis of target parameters estimation using multiple widely separated antenna arrays," *IEEE Trans. Aerosp. Electron. Syst.*, vol. 52, no. 5, pp. 2413–2435, Oct. 2016.
[50] A. Sakhnini, M. Guenach, A. Bourdoux, and S. Pollin, "A Cramér-Rao lower bound for analyzing the localization performance of a multistatic joint radar-communication system," in *Proc. 1st IEEE Int. Online Symp. Joint Commun. Sens.*, 2021, pp. 1–5.
[51] S. K. Dehkordi, L. Pucci, P. Jung, A. Giorgetti, E. Paolini, and G. Caire, "Multistatic parameter estimation in the near/far field for integrated sensing and communication," *IEEE Trans. Wireless Commun.*, vol. 23, no. 12, pp. 17929–17944, Dec. 2024.
[52] F. Liu, L. Zhou, C. Masouros, A. Li, W. Luo, and A. Petropulu, "Toward dual-functional radar-communication systems: Optimal waveform design," *IEEE Trans. Signal Process.*, vol. 66, no. 16, pp. 4264–4279, Aug. 2018.
[53] F. Liu, Y. -F. Liu, A. Li, C. Masouros, and Y. C. Eldar, "Cramér-Rao bound optimization for joint radar-communication beamforming," *IEEE Trans. Signal Process.*, vol. 70, pp. 240–253, 2022.
[54] F. Zabini, E. Paolini, W. Xu, and A. Giorgetti, "Joint sensing and communications in finite block-length regime," in *Proc. IEEE Glob. Commun. Conf.*, 2022, pp. 5595–5600.
[55] M. A. Islam, G. C. Alexandropoulos, and B. Smida, "Integrated sensing and communication with millimeter wave full duplex hybrid beamforming," in *Proc. IEEE Int. Conf. Commun.*, 2022, pp. 4673–4678.
[56] I. Gavras, M. A. Islam, B. Smida, and G. C. Alexandropoulos, "Full duplex holographic MIMO for near-field integrated sensing and communications," in *Proc. Eur. Signal Proc. Conf.*, 2023, pp. 700–704.
[57] M. Talha, B. Smida, M. A. Islam, and G. C. Alexandropoulos, "Multi-target two-way integrated sensing and communications with full duplex MIMO radios," in *Proc. Asilomar Conf. Signals, Syst., Comput.*, 2023, pp. 1661–1667.
[58] M. S. Greco, P. Stinco, F. Gini, and A. Farina, "Cramér-Rao bounds and selection of bistatic channels for multistatic radar systems," *IEEE Trans. Aerosp. Electron. Syst.*, vol. 47, pp. 2934–2948, Oct. 2011.
[59] I. Pasya, N. Iwakiri, and T. Kobayashi, "Joint direction-of-departure and direction-of-arrival estimation in a UWB MIMO radar detecting targets with fluctuating radar cross sections," *Int. J. Antennas Propag.*, vol. 2014, 2014, Art. no. 847815.
[60] H. Jiang, J.-K. Zhang, and K. M. Wong, "Joint DOD and DOA estimation for bistatic MIMO radar in unknown correlated noise," *IEEE Trans. Veh. Technol.*, vol. 64, no. 11, pp. 5113–5123, Nov. 2015.
[61] L. Pucci, E. Matricardi, E. Paolini, W. Xu, and A. Giorgetti, "Performance analysis of a bistatic joint sensing and communication system," in *Proc. IEEE Int. Conf. Commun. Workshops*, 2022, pp. 73–78.
[62] L. G. de Oliveira et al., "Bistatic OFDM-based joint radar-communication: Synchronization, data communication and sensing," in *Proc. 20th Eur. Radar Conf.*, 2023, pp. 359–362.
[63] X. Zhang, Y. Ma, Y. Zeng, S. Sun, and Y. Wang, "Bistatic joint radar and communication with 5G signal for range speed angle detections," in *Proc. IEEE 98th Veh. Technol. Conf.*, 2023, pp. 1–5.
[64] Q. Zhao, A. Tang, X. Wang, J. Liu, Y. Zhou, and F. Gao, "Joint transmit and receive beamforming for integrated bistatic radar sensing and MU-MIMO communications," in *Proc. IEEE 98th Veh. Technol. Conf.*, 2023, pp. 1–6.
[65] M. A. Richards, *Fundamentals of Radar Signal Processing*. New York, NY, USA: McGraw-Hill, 2005.
[66] S. M. Kay, *Fundamentals of Statistical Signal Processing: Estimation Theory*. Englewood Cliffs, NJ, USA: Prentice-Hall, 1993.

Flavio Zabini (Member, IEEE) received the Laurea (*summa cum laude*) in telecommunications engineering and the Ph.D. degree in electronic engineering and computer science from the University of Bologna, Bologna, Italy, in 2004 and 2010, respectively. In 2004, he developed his master's thesis with the University of California San Diego, La Jolla, CA, USA. In 2008, he was a Visiting Student with the DoCoMo Eurolabs of Munich, Munich, Germany. From 2013 to 2014, he was a Postdoctoral Fellow with the German Aerospace Center, Cologne, Germany. He was with the IEIIT-Bo of CNR. He is currently an Associate Professor with the University of Bologna. His research interests include stochastic sampling, molecular communications, and joint sensing and communications. He was an Associate Editor for the IEEE COMMUNICATION LETTERS and *KSII Transactions on Internet and Information Systems*.

Andrea Giorgetti (Senior Member, IEEE) received the Dr.-Ing. degree (*summa cum laude*) in electronic engineering and the Ph.D. degree in electronic and computer engineering from the University of Bologna, Bologna, Italy, in 1999 and 2003, respectively. From 2003 to 2005, he was a Researcher with the National Research Council of Italy. In 2006, he joined the Department of Electrical, Electronic, and Information Engineering "Guglielmo Marconi," University of Bologna, as an Assistant Professor and became an Associate Professor in 2014. In 2006, he was also with the Laboratory for Information and Decision Systems, Massachusetts Institute of Technology, Cambridge, MA, USA. His research interests include ultra-wideband communication systems, wireless sensor networks, cognitive radio, localization, and integrated sensing and communications. From 2017 to 2018, he was the Elected Chair of the IEEE Communications Society's Radio Communications Technical Committee. He is the former Editor of the IEEE COMMUNICATIONS LETTERS and IEEE TRANSACTIONS ON WIRELESS COMMUNICATIONS.